P-14-06

SR-PSU Hydrogeological modelling

TD13 – Periglacial climate conditions

Patrik Vidstrand, TerraSolve AB

Sven Follin, SF GeoLogic AB

Johan Öhman, Geosigma AB

December 2014

Svensk Kärnbränslehantering AB
Swedish Nuclear Fuel
and Waste Management Co

Box 250, SE-101 24 Stockholm
Phone +46 8 459 84 00

ISSN 1651-4416
SKB P-14-06
ID 1399522

SR-PSU Hydrogeological modelling

TD13 – Periglacial climate conditions

Patrik Vidstrand, TerraSolve AB

Sven Follin, SF GeoLogic AB

Johan Öhman, Geosigma AB

December 2014

Keywords: Hydrogeology, Bedrock, Modelling, Periglacial, Forsmark, SFR, Safety assessment.

Preface

The work presented in the current report describes the periglacial parts of the hydrogeological modelling for the fractured crystalline rock (bedrock) at the Forsmark-SFR site carried out as part of the SR-PSU project.

Patrik Vidstrand

Abstract

As a part of the license application for an extension of the existing repository for short-lived low and intermediate radioactive waste at the Forsmark-SFR site, the Swedish Nuclear Fuel and Waste Management Company (SKB) has undertaken site-scale groundwater flow modelling studies. The studies have been carried out within the SR-PSU project and represent two different climate domains; temperate and periglacial. Periods with Glacial climate conditions are not a part of the hydrogeological modelling in SR-PSU for reasons described in Odén et al. (2014). The groundwater flow simulations carried out contribute to the overall evaluation of the radiological safety of the geological disposal of short-lived low and intermediate radioactive waste in the bedrock at the Forsmark-SFR site.

The present report describes the groundwater flow modelling methodology, assessed data, setup, and results. It is the primary reference for the conclusions drawn in a SR-PSU-specific context concerning groundwater flow in the bedrock during the assessed periglacial climate conditions.

Sammanfattning

Som en del av ansökan för ett utbyggt SFR har Svensk Kärnbränslehantering (SKB) genomfört olika grundvattenmodelleringsstudier. Studierna har utförts inom projekt SR-PSU och hanterar grundvattenströmning under perioder med två olika klimatförhållanden; tempererade och periglaciala. Inga studier av grundvattenströmning under perioder med glaciala förhållanden behövs inom SR-PSU (se Odén et al. 2014). Beräkningsresultaten från de utförda simuleringarna ingår i bedömningsunderlaget inom design och långsiktig säkerhet.

Föreliggande rapport sammanfattar modelleringsstudiernas uppställning, använd data, genomförande och resultat. Rapporten utgör huvudreferens för SR-PSU vad gäller resultat som är kopplade till grundvattenströmning under de studerade periglaciala klimatförhållandena.

Contents

1 Introduction

As a part of the license application for SFR 3, the Swedish Nuclear Fuel and Waste Management Company (SKB) initiated the SFR extension project (PSU). In SR-PSU the radiological safety for the entire SFR-repository after closure is addressed. A site descriptive model, SDM-PSU (SKB 2013) was developed to describe the hydrogeological setting at SFR. More or less the same flow model is applied in SR-PSU, as a numerical tool to assess the performance of a backfilled repository. Two different climate domains are studied in SR-PSU (temperate and periglacial domains; Odén et al. 2014).

All groundwater-flow modelling tasks within SR-PSU are strictly defined by means of so-called Task Descriptions (TDs). This document describes the model results of tasks defined in TD13, including input-data handling, numerical setup of model cases, simulation procedures, as well as, handling of output. TD13 assesses the impact of periglacial climate conditions, by means of a sensitivity analysis for three selected bedrock cases.

2 TD 13 description

2.1 Context and approach

The groundwater flow model developed within SDM-PSU and SR-PSU follows the system approach described in Rhén et al. (2003) and consists of three conceptual hydrogeological units:

- HSD (Hydraulic Soil Domain), representing the regolith, i.e. any loose material covering the bedrock, e.g. Quaternary deposits, artificial filling material, and weathered rock,
- HCD (Hydraulic Conductor Domain), representing deformation zones, and
- HRD (Hydraulic Rock mass Domain), representing the less fractured bedrock in between the deformation zones.

The uncertainty in HRD is modelled by means of stochastic discrete-fracture network (DFN) realisations. The assessed HCD parameterisation involves two components of variability: 1) heterogeneity and 2) conceptual uncertainties. In the permafrost scenarios three of these realisations are assessed, representing the range of uncertainty as defined in the temperate climate modeling (Öhman et al. 2014). Another model complexity concerns the shoreline retreat and altering flow regime during the time span addressed; in SR-PSU the permafrost scenario focus on the time period of 17,000 AD and as such uses a shoreline location much different from present day conditions (–57.4 metres below present day shoreline).

When studying past influences of periglacial and glacial conditions on the hydrogeological evolution of a site, boundary conditions derived from climate constraints are needed. This, in turn, needs to be based on a reconstruction of the paleoclimatic evolution or a projected future evolution. In the SR-PSU safety assessment (SKB 2014a), paleoclimate and environmental conditions were reconstructed for the last glacial cycle (SKB 2014b). The reconstruction consists of a 120,000 years long succession of three general climate domains relevant for Fennoscandia; that is temperate, periglacial, and glacial climate domains. The future projections consist of 100,000 years succession of two general climate domains, that is temperate and periglacial. In addition, the reconstruction also describes periods with submerged conditions, occurring after major glacial phases due to isostatic depression of the crust and to sea level changes. Figure 2-2 illustrates, from a hydrogeological perspective, the conceptual models of the climate domains relevant for the Forsmark area. Based on these conceptual models, the numerical groundwater model is developed in order to contain all essential processes, governing the recharge and discharge of water at the top boundary.

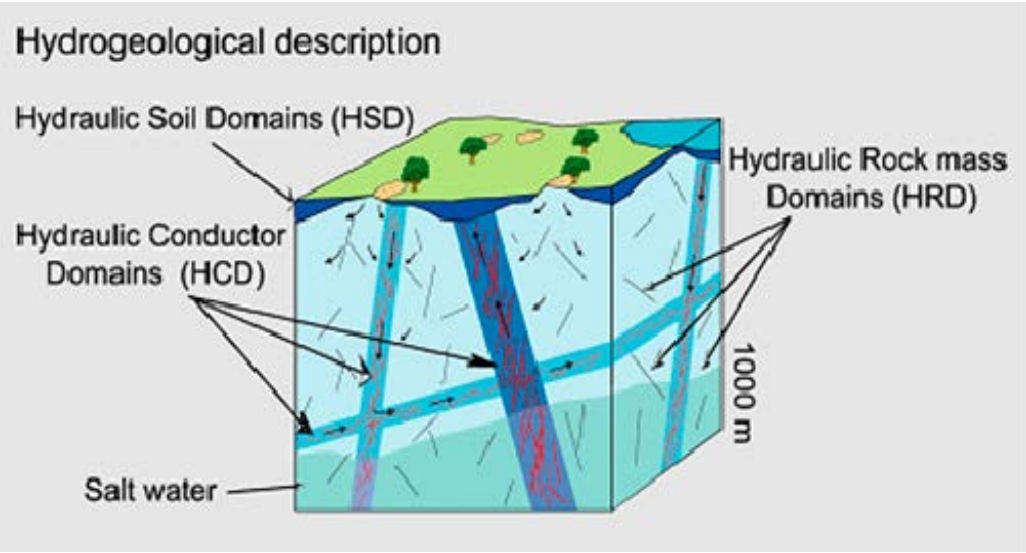

Figure 2-1. *Cartoon showing the division of the crystalline bedrock and the regolith (Quaternary deposits) into three hydraulic domains, HCD, HRD and HSD. (Source: Rhén et al. 2003, Figure 3-2.)*

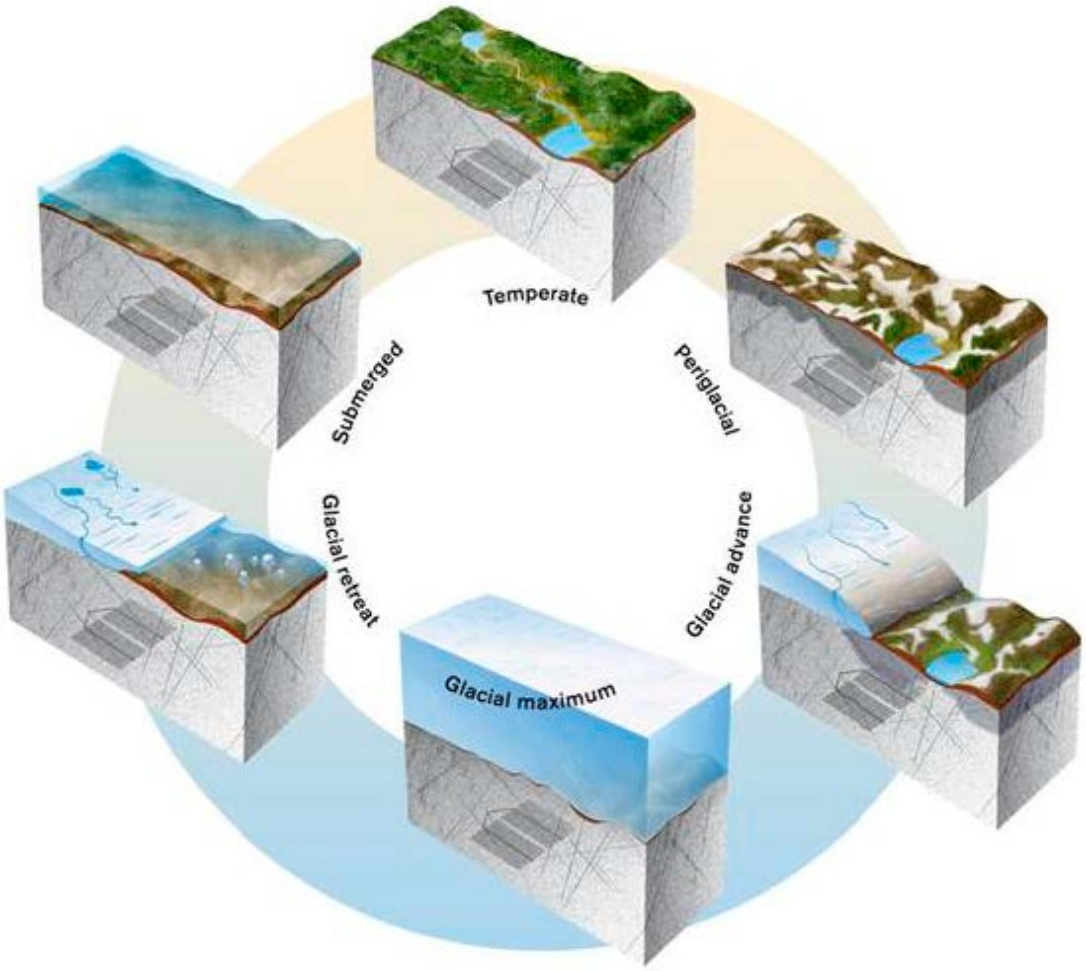

Figure 2-2. *Conceptual illustration of the hydrological system for different climate domains.*

The scope of work assessed in the permafrost scenarios are:

- Calculate through flow, total and local values, to SFR 1 and SFR 3 layout using the SFR regional flow model area.
- Calculate discharge locations for particle traces passing through repository vaults in SFR 1 and the SFR 3 layout using the SFR flow model area.
- Calculate the pressure field in the near-field of SFR. Calculate permafrost-associated property changes in the near-field of SFR.
- Calculate relevant performance measures, e.g. Darcy fluxes, flow-related transport resistance, path length, and advective travel time.

The simulations are TH coupled and permafrost is studied by means of two variants where the fozen ground reaches 1) elevations just above SFR 1, 2) reach elevations between SFR 1 and the SFR 3 layout.

2.2 Objectives

The main objective in TD13 is to analyse the impact of uncertainty in flow conditions at SFR 1 and SFR 3 due to different climate conditions in terms of the defined performance measures. This is evaluated by means of a sensitivity analysis for three selected bedrock cases and variants in climate conditions. The sensitivity analysis concerning bedrock properties only addresses parameterisation variants inside the SFR regional domain (Figure 4-1); outside, the properties are kept fixed.

The impact of the assessed uncertainty is evaluated in terms of:

1) Flow through disposal facilities (existing SFR 1 and the planned extension SFR 3).

2) Flow path properties (quantified by means of particle tracking).

Results are delivered to the other modelling teams in SR-PSU (near-field modelling, biosphere modelling, chemical modelling, and radionuclide transport modelling), according to the specifications in [TD13] (Appendix A).

Based on the outcome of the groundwater flow simulations during temperate climate conditions, three bedrock cases were selected to characterise the observed range of heterogeneity and conceptual uncertainty in bedrock parameterisation. The three bedrock cases were selected based on calculated cross flows through the eleven rock vaults in SFR 1 and SFR 3. They comprised the following.

1. One "low-flow" bedrock case: bedrock parameterisation variant with low disposal-facility cross flows.
2. A "base case" bedrock case: a bedrock parameterisation variant with median disposal-facility cross flows.
3. One "high-flow" bedrock case: a bedrock parameterisation variant with high disposal-facility cross flows.

These bedrock cases are used in the groundwater flow modelling during periglacial climate conditions, with additional parameterisations specific for permafrost modelling.

The uncertainty in climate conditions is investigated via a combination of two types of top boundary conditions 1) depth of permafrost and 2) landscape or surface variants.

To cover the uncertainty in the future climate evolution in Forsmark (SKB 2014b), the depth of permafrost is simulated with three alternatives:

- Shallow permafrost (reaching depths of approximately –60 m elevation).
- Deep permafrost reaching depths within SFR 1 (about –85 m elevation).
- Deep permafrost reaching depths beneath SFR 1 (about –90 m elevation).

Also the landscape is studied by variants and is simulated using three alternatives. These variants primarily investigate the possibility of a situation where peat bogs and small ponds are kept unfrozen, that could be possible initially for a periglacial condition, further the effect of unfrozen streams are investigated. The future streams at Forsmark are narrow and not expected to be a large source of heat, also the gridding of the surface exaggerate the stream in width yielding a too wide unfrozen surface layer. These uncertainties are investigated by a variant assuming streams as a positive temperature boundary as well as a negative temperature boundary. The landscape variants are:

1. "All" superficial water bodies (ponds, peat bogs, streams and lakes).
2. Lakes and streams only.
3. Lakes only.

Different combinations of these top boundary conditions are applied.

2.3 Computational code

The groundwater flow modelling in SR-PSU used version 3.4 of the DarcyTools computational code (Svensson et al. 2010). This version of DarcyTools contains an algorithm that is used to simulate changes in the permeability due to freezing and thawing. Changes of the groundwater salinity due to freezing and thawing are not considered. The heat flux from the repository to the surface is also omitted. In total, the model domain consists of approximately 4.7 million cells.

2.4 Setting of Forsmark

The Forsmark area is located in northern Uppland within the municipality of Östhammar, about 120 km north of Stockholm. The Forsmark area consists of crystalline bedrock that belongs to the Fennoscandian Shield, one of the ancient continental nuclei of the Earth. The bedrock at Forsmark in the south-western part of this shield formed between 1.89 and 1.85 billion years ago during the Svecokarelian orogeny. It has been affected by both ductile and brittle deformation. The ductile deformation has resulted in large-scale, ductile high-strain belts and more discrete high-strain zones. Tectonic lenses, in which the bedrock is less affected by ductile deformation, are enclosed between the ductile high strain belts.

The current ground surface in the Forsmark region forms a part of the sub-Cambrian peneplain in south-eastern Sweden. This peneplain comprises a relatively flat topographic surface with a gentle dip towards the east that formed more than 540 million years ago. The whole area is located below the highest coastline associated with the last glaciation, and large parts of the candidate area emerged from the Baltic Sea only during the last 2,000 years. Both the flat topography and the still on-going shore-level displacement of c. 6mm per year strongly influence the current landscape. Sea bottoms are continuously transformed into new terrestrial areas or freshwater lakes, and lakes and wetlands are successively in-filled by peat.

2.5 Model cases

The permafrost simulations are variants based on different bedrock cases and different climate conditions. The assessed bedrock cases are described in Table 2-1 while the different climate set-ups are given in Table 2-2 and Table 2-3. The complete set of model cases is given in Table 2-4.

Table 2-1. Bedrock cases assessed in permafrost variants. Used numbers (No.) are the same as in TD11 (Öhman et al. 2014).

No.	Label	HCD Conditioning	Depth trend	Variability	HRD
1	BASE_CASE1_DFN_R85	Yes	Yes	Homogeneous	R85
11	nc_DEP_R07_DFN_R85	No	Yes	Heterogeneous, R07	R85
15	nc_NoD_R01_DFN_R18	No	No	Heterogeneous, R01	R18

Table 2-2. Climate set-ups assessed in the permafrost simulations. Ground temperatures, in the so called column, represent the simulated fixed temperature boundary for a specified time (i.e. simulated time) given in the column: Time.

No.	Label	Temperature boundary Ground temperature (°C)	Time (years)
1	Shallow permafrost	–2	200
2	Within SFR 1	–4	200
3	Beneath SFR 1	–4	250

Table 2-3. Assessed surface (landscape) variants of climate set-ups in the permafrost simulations.

No.	Label	Water bodies Ponds	Lakes	Rivers
1	Extensive water bodies	Yes	Yes	Yes
2	Lakes and Rivers	No	Yes	Yes
3	Lakes	No	Yes	No

Table 2-4. Assessed model cases in the permafrost simulations.

Simulation	Case	Bedrock case	Permafrost depth	Surface objects
0	BaseCase Pressure	1	–	–
1	Case_1_1_1	1	Above SFR 1	All
2	Case_1_2_1	1	Within SFR 1	All
3	Case_1_3_1	1	Below SFR 1	All
4	Case_11_1_1	11	Above SFR 1	All
5	Case_11_2_1	11	Within SFR 1	All
6	Case_11_3_1	11	Below SFR 1	All
7	Case_15_1_1	15	Above SFR 1	All
8	Case_15_2_1	15	Within SFR 1	All
9	Case_15_3_1	15	Below SFR 1	All
10	Case_1_1_2	1	Above SFR 1	Lakes and streams
11	Case_1_2_2	1	Within SFR 1	Lakes and streams
12	Case_1_3_2	1	Below SFR 1	Lakes and streams
13	Case_11_1_2	11	Above SFR 1	Lakes and streams
14	Case_11_2_2	11	Within SFR 1	Lakes and streams
15	Case_11_3_2	11	Below SFR 1	Lakes and streams
16	Case_15_1_2	15	Above SFR 1	Lakes and streams
17	Case_15_2_2	15	Within SFR 1	Lakes and streams
18	Case_15_3_2	15	Below SFR 1	Lakes and streams
19	Case_1_1_3	1	Above SFR 1	Lakes
20	Case_1_2_3	1	Within SFR 1	Lakes
21	Case_1_3_3	1	Below SFR 1	Lakes
22	Case_11_1_3	11	Above SFR 1	Lakes
23	Case_11_2_3	11	Within SFR 1	Lakes
24	Case_11_3_3	11	Below SFR 1	Lakes
25	Case_15_1_3	15	Above SFR 1	Lakes
26	Case_15_2_3	15	Within SFR 1	Lakes
27	Case_15_3_3	15	Below SFR 1	Lakes

It is noted that all cases have been simulated however the reporting will focus on results only deemed relevant to explain the impact of climate uncertainty.

2.6 Hydraulic conditions during permafrost

Permafrost is present if the ground temperature is at or below 0°C for at least two consecutive years (e.g. French 1996, Lemieux et al. 2008b). The greatest impact of permafrost on the subsurface hydrology is the phase change related to the freezing of groundwater. Permafrost is often imagined to create an almost impervious (small, but still nonzero permeability) layer near the surface, which decreases the potential groundwater recharge and discharge, highlighting the possibility of high groundwater pressures beneath the permafrost layer (e.g. Burt and Williams 1976, Kleinberg and Griffin 2005, Bense and Person 2008, Lemieux et al. 2008a, b, c).

The above definition of permafrost does not imply that the surface is completely frozen, however. Due to capillary forces, water does not freeze completely and a thin film of liquid water covers the rock/soil grains even at low temperatures (Kane and Stein 1983, Gascoyne 2000, Vidstrand 2003). The unfrozen water content under permafrost conditions is sufficient to maintain the groundwater table at or close to the surface (Person et al. 2007). In this context, the occurrence of taliks[1] is considered to be an important top boundary condition (e.g. McEwen and de Marsily 1991, Boulton et al. 1993, Haldorsen and Heim 1999).

[1] Taliks are unfrozen “holes” in the permafrost layer that can if the taliks are open, that is unfrozen condition exist between the surface and the deeper parts of the geosphere, connect the flow system at depth with that close to the surface. Taliks have been observed below large surface water bodies, even where the permafrost is quite deep in the surrounding regions (Lemieux et al. 2008b, Johansson et al. 2014).

Physical permafrost models, which are based on the state equations for the phase change, suggest large variations in the unfrozen water content, and hence also in the hydraulic conductivity and transport properties, depending on the temperature and the geological material. Burt and Williams (1976) and Kleinberg and Griffin (2005) provide some information about the field permeability of soils as a function of the unfrozen water content, but, on the whole, there are few field data reported in the literature. As a consequence, the choice of model parameters is often based on laboratory experiments (e.g. Williams and Smith 1989).

2.7 Modelling sequence

The permafrost simulations are numerical demanding and need a complex series of time steps in order to reach numerical convergence. The complexity of different rock properties, such as of thermal and hydraulic, makes the model sensitive; furthermore, the soil domain complexity adds large heterogeneity within the property field, thus making the models even more sensitive. In order to maintain the detailed description a series of time stepping simulations was constructed.

First a model with 50 time steps of 1 year each was simulated using 20 sweeps (staggered coupling of the processes); each sweep include iterations until a specified convergence criteria was reached. Typically these first 50 steps took 10 days of CPU. Restarting the results of this first model with 3 time steps of 50 years using 30 sweeps; each sweep include iterations until a specified convergence criteria was reached. Typically these three steps took 2 days of CPU.

Restarting the results from the second model with time steps of 1 day was done in order to produce post-processed results for other modelling tools. These simulations take on average less than 1 hour.

3 Concepts and methodology

In permafrost simulation one needs to account for the phase change of water when the temperature drops below freezing, the mass conservation equation and the heat transport equation have to be modified. Also properties such as permeability and thermal conductivity need to be modified to account for the freezing.

In reality frozen ground is a four-phase system consisting of intact rock (however with some porosity), frozen fluid (ice), unfrozen fluid (e.g. water) and gases (e.g. air). Assuming that the pore space of the groundwater system is unchanged and filled with either ice or water, that is ignoring the possibility of a gaseous phase and simply adding the ice phase to a single fluid phase, a simplified ice content function ε is employed:

$$\phi_i = \varepsilon\phi$$
$$\phi_f = (1-\varepsilon)\phi \qquad \text{Eq 3-1}$$

where ϕ is the total kinematic porosity [–], ϕ_i is the part of the kinematic porosity filled with ice, ϕ_f the part filled with water, and ε represents the ice content function. ε is generally assumed a continuous function of temperature and is given by:

$$\varepsilon = \varepsilon_{\max}\left(1-\exp(-\beta_e)\right)$$
$$\beta_e = \left(\frac{\min\{T, T_L\} - T_L}{w}\right)^2 \qquad \text{Eq 3-2}$$

where ε_{max} is the maximum value (generally assumed as 1), T_L is the thawing temperature, and w is a thawing interval which has to be adopted to the simulated ground conditions (material) herein specified to 1 for a good approximation of bedrock.. The freezing temperature is fixed to 0°C independent of pressure and salinity. The shallow location of the SFR facility, and the fact that no glacial conditions are accounted for, make these omissions valid. The freezing/thawing interval is specified to occur over one degree, primarily trimmed to yield as good an approximation as possible of the general bedrock.

In the present study, the permeability is assumed to be reduced by a power function of the unfrozen water content:

$$k = \alpha k_{ref} \qquad \text{Eq 3-3}$$

with:

$$\alpha = \max(\alpha_{min}, (1-\varepsilon)^a \qquad \text{Eq 3-4}$$

where the subscript '$_{ref}$' indicates the reference values associated with unfrozen conditions and α_{min} is a specified maximum reduction, herein assigned to five orders of magnitude. It is noted that no information on α typical for fractured crystalline rocks has been found in the literature. Relations between temperature and hydraulic conductivity for different saturated frozen soils (typically silt and sand materials) are reported by Burt and Williams (1976). In this reference most of the tested materials seem to reach a plateau when approaching hydraulic conductivity values between $1\cdot10^{-11}$ m/s and $1\cdot10^{-13}$ m/s; i.e. the hydraulic conductivity does not seem to be further reduced with lower temperatures. Similar experimental data are also presented in Kleinberg and Griffin (2005).

The introduction of an ice phase dependent on the temperature links the conservation equations, which become non-linear. When the densities of the solid (ice) and fluid phase differs, there is a motion of the fluid due to changes in volumes. Incorporating these effects yields a mass conservation equation as follows:

$$\frac{\partial \rho_f \phi}{\partial t} + \frac{\partial (\rho_i - \rho_f)\varepsilon\phi}{\partial t} + \frac{\partial}{\partial x}(\rho_f u) + \frac{\partial}{\partial y}(\rho_f v) + \frac{\partial}{\partial x}(\rho_f w) = Q \qquad \text{Eq 3-5}$$

where ρ_f is fluid density [ML^{-3}], ρ_i is ice density [ML^{-3}], t is time [T] (u, v, w) are the directional components of the volumetric (Darcy) flux **q** [LT^{-1}] at the location (x, y, z) [L,L,L] in a Cartesian coordinate system, and Q is a source/sink term per unit volume of fluid mass [$ML^{-3}T^{-1}$]. The mass conservation equation is turned into a pressure equation by invoking the assumptions behind Darcy's law:

$$\begin{aligned} u &= -\frac{k_x}{\mu}\frac{\partial P}{\partial x} \\ v &= -\frac{k_y}{\mu}\frac{\partial P}{\partial y} \\ w &= -\frac{k_z}{\mu}\frac{\partial P}{\partial z} - \frac{k_z}{\mu}(\rho_f - \rho_0)g \end{aligned} \qquad \text{Eq 3-6}$$

where k_x, k_y and k_z are the orthogonal components of the permeability tensor parallel to the Cartesian coordinate system [L^2], μ is the fluid dynamic viscosity [$ML^{-1}T^{-1}$], g is the acceleration due to gravity [LT^{-2}], ρ_0 is a reference fluid density [ML^{-3}], and P is the residual (dynamic) fluid pressure [$ML^{-1}T^{-2}$] at the location (x, y, z):

$$P = p + \rho_0 gz \qquad \text{Eq 3-7}$$

where p is the gauge pressure [$ML^{-1}T^{-2}$] and $\rho_0 gz$ is the hydrostatic pressure, P_0.

The hydraulic conductivity K [LT^{-1}] is related to the permeability k through the relation:

$$K = \frac{\rho_f\, g}{\mu} k \qquad \text{Eq 3-8}$$

Under temperate conditions within the depth interval the SFR facility is located in, state laws could be viewed as independent of temperature. However, in the periglacial climate condition much of the flow occurs around temperatures below or close to 0°C, a temperature interval in which the state laws are more sensitive.

In the performed simulations the state laws governing density and viscosity have been made dependent on temperature trimmed to fit the temperature interval between 0 and 20°C.

For variable-density flow at isothermal conditions, ρ_f and μ are given by the following state laws:

$$\rho_f = \rho_0\left[1 + \alpha_1 C + \alpha_2 C^2 - \beta_1(\theta - \theta_0) - \beta_2(\theta - \theta_0)^2\right] \qquad \text{Eq 3-9}$$

$$\mu = \mu_0\left[1 + \alpha_3 C + \alpha_4 C^2 + \beta_3(\theta - \theta_0) + \beta_4(\theta - \theta_0)^2\right]^{\gamma} \qquad \text{Eq 3-10}$$

where α, β γ and μ_0 are constants and C and θ represent the salinity (mass fraction) [–], herein the salinity is specified as zero, and the temperature [K] with θ_0 set as zero degrees C.

Herein the parameters are given as:

ρ_0	α_1	α_2	β_1	β_2
1,000	$7.80\cdot10^{-3}$	$-1.18\cdot10^{-4}$	$5.73\cdot10^{-5}$	$3.70\cdot10^{-6}$

μ_0	α_3	α_4	β_3	β_4	γ
$1.78\cdot10^{-3}$	$7.80\cdot10^{-3}$	$-1.18\cdot10^{-4}$	$-2.25\cdot10^{-2}$	$1.67\cdot10^{-4}$	1.3

The heat conservation equation may be written as:

$$\rho\phi\frac{\partial c_{pf}\theta}{\partial t}+\frac{\partial(1-\phi)c\ \theta}{\partial t}+\frac{\partial\phi c_i\theta}{\partial t}-\rho_i L\frac{\partial\varepsilon}{\partial\theta}\phi\frac{\partial\theta}{\partial t}$$
$$+\frac{\partial}{\partial x}\left(\rho_f u c_{pf}\theta-\lambda_x\frac{\partial\theta}{\partial x}\right)$$
$$+\frac{\partial}{\partial y}\left(\rho_f v c_{pf}\theta-\lambda_y\frac{\partial\theta}{\partial y}\right) \qquad \text{Eq 3-11}$$
$$+\frac{\partial}{\partial z}\left(\rho_f w c_{pf}\theta-\lambda_z\frac{\partial\theta}{\partial z}\right)=\left(\frac{\partial\rho_f u}{\partial x}+\frac{\partial\rho_f v}{\partial y}+\frac{\partial\rho_f w}{\partial z}\right)c_{pf}\theta+Q_T$$

with:

$$c_i = \rho_i(c_{pi}-c_{pf})\varepsilon \qquad \text{Eq 3-12}$$

where ε is given by Eq. 3-1, ρ is described by Eq. 3-11, θ is the temperature [K], c_{pf} is the specific heat capacity of the fluid and c_{pi} is the specific heat capacity of ice [$L^2T^{-2}K^{-1}$] (or [J/(kg K)]), c is the specific heat capacity of the ground [$L^2T^{-2}K^{-1}$] (or [J/(kg K)]), L is the specific latent heat [L^2T^{-2} (or J/kg)], and λ_x , λ_y, and λ_z are the orthogonal components of the equivalent (i.e. matrix with fluid) thermal conductivity tensor [$MLT^{-3}K^{-1}$] (or [W/(m K)]). Q_T represents a sink/source term [$ML^{-1}T^{-3}$] ([or W/m^3]).

The individual phases are assumed randomly distributed within a unit volume and, hence, the thermal conductivity is computed as a mean square root weighting of the three phases' (matrix, fluid, ice) individual thermal conductivities. However, as the thermal conductivity of the matrix is not directly used, but instead the equivalent thermal conductivity of the unfrozen material, the thermal conductivity of frozen ground is computed as:

$$\lambda = (\sqrt{\lambda_{ref}} + (\sqrt{\lambda_i} - (\sqrt{\lambda_f})\varepsilon\phi)^2 \qquad \text{Eq 3-13}$$

where λ_{ref} is the equivalent thermal conductivity of the saturated matrix, λ_i is the ice thermal conductivity and λ_f is the thermal conductivity of the fluid.

4 Geometrical data

4.1 Model domains

The model domains used in the permafrost modelling are the same as the ones used in the temperate modelling (Öhman et al. 2014). Below only a summary of sections deemed essential is given.

4.1.1 Flow domain

The flow domain defines the outer perimeter of the model volume (Figure 4-1). The vertical sides of the model have no-flow boundary conditions in all simulations; hence the flow domain is defined based on topographical water divides. Areas that are currently below sea are chosen with respect to: 1) modelled future topographical divides in RLDM, 2) the deep Seafloor trench (the so-called Gräsörännan), and 3) general expectations of the regional future hydraulic gradient. The flow domain extends vertically from surface elevations (in general between +25 and –25 m) to –1,100 m elevation.

4.1.2 SFR regional domain

The regional-scale model volume has a key role in the sensitivity analysis, as the bedrock parameterisation variants are geometrically confined to the volume inside the SFR regional domain. The bedrock properties outside this domain are kept fixed in all simulations. Consequently, the SFR regional domain is a central geometric boundary for merging two types of bedrock parameterization: 1) developed within the SR-PSU/SDM-PSU project inside the SFR regional domain, addressed by bedrock cases, with 2) developed in the SDM-Site/SR-Site Forsmark outside this domain. The SFR regional domain also controls grid generation and defines the boundaries for DFN generation. The coordinates defining the horizontal extent of the model volumes are provided in Table 4-1.

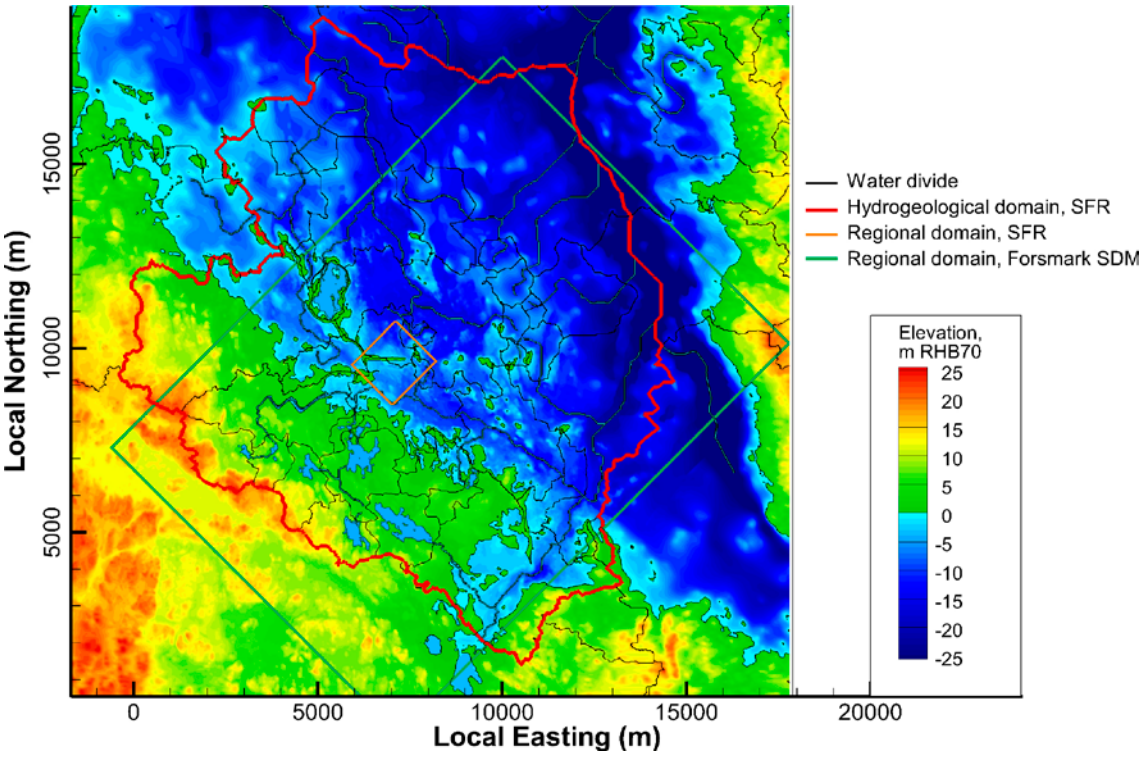

Figure 4-1. The flow domain (red line) is the outer boundary in the model. The SFR regional domain (orange polygon in centre area) is the boundary for bedrock parameterization variants; hence no variability in hydrogeological properties is investigated outside the SFR regional domain.

Table 4-1. Coordinates defining model areas for SFR. RT90 (RAK) system.

Regional model volume		Local model volume	
Easting (m)	Northing (m)	Easting (m)	Northing (m)
1631920.0000	6701550.0000	1632550.0000	6701880.0000
1633111.7827	6702741.1671	1633059.2484	6702388.9854
1634207.5150	6701644.8685	1633667.2031	6701780.7165
1633015.7324	6700453.7014	1633157.9547	6701271.7311

Based on the defined coordinates, a DarcyTools object [SFR_modellområde_v01.dat] was constructed. The object is rotated into the local DarcyTools coordinate system [R_SFR_modellområde_v01.dat] by means of the Fortran code [Rotate_DT_objects.f90]. Pivot point in local coordinate system: [6400. 9200.], rotation angle: 32.58816946°.

4.2 Tunnel geometry

The tunnel geometries used in the permafrost modeling are the same as the ones used in the temperate modelling (Öhman et al. 2014). Below only a summary of sections deemed essential is given.

Tunnel and tunnel plug geometry is defined in CAD (PP: _24_SFR_STL_121220). The CAD data set contains: 1) the existing SFR 1, 2) the planned extension of SFR (SFR 3), and 3) planned tunnel plug geometries. The data set corresponds to alternative L1BC in TD10 (SKBdoc 1395215), but has been updated in three aspects:

1) Revised geometric definitions of plugs (i.e. some plug geometries have been updated, since TD10).
2) Fix bugs that were discovered in the TD10 delivery (i.e. using geometrical data to classify grid-cell functionality: backfill/plug/bedrock/particle-release locations, etc in the DarcyTools model requires that the source CAD objects are defined as watertight solids).
3) The geometric definition of the disposal facility 2BMA has been modified slightly.

These geometric tunnel data have two functions in grid generation: 1) to control local grid refinement, and 2) to define grid cells in different tunnel sections, by means of so-called "DarcyTools cell markers". In effect, the tunnel data can be said to have 4 central functions in the flow modelling:

1) Local grid refinement: tunnel cells have a maximum side length of 2 m.

2) Parameterisation: so-called "DarcyTools cell markers" are used to identify the different types of back-fill material in tunnel cells, which is used to set hydraulic properties.

3) Particle-release points: defined as the entire volume of disposal facilities (yellow volumes in Figure 4-2; note that Silo barriers are not included). Particle-release points are also identified via DarcyTools cell markers.

4) Tunnel flow: defined as net flow over tunnel walls. Likewise, DarcyTools cell markers are used to identify tunnel walls of disposal facilities.

The tunnel related geometries are delivered as 3D CAD volumes, which are converted into DarcyTools objects by means of the DarcyTools module OGN. The objects are rotated into the local DarcyTools coordinate system by means of the Fortran code [Rotate_DT_objects.f90]. Pivot point in local coordinate system: [6400. 9200.], rotation angle: 32.58816946°.

The implementation of tunnel geometry (Figure 4-2) into the DarcyTools computational grid requires processing of delivered data (Table B-1 in Appendix B):

1) All geometric tunnel data (original CAD format *.stl) are converted into the so-called DarcyTools-object format (changing file extension to *.dat). Filenames of DarcyTools objects are shortened, as DarcyTools has an upper limit of 32 characters in object names. Typically, the substrings "SFR1", "L1BC", and "plugg" can be omitted (filename traceability via Table 4-2).
2) All geometrical objects (*.dat) are translated and rotated into the local model coordinate system (adding the prefix "R_"*.dat) (Table B-2 in Appendix B).

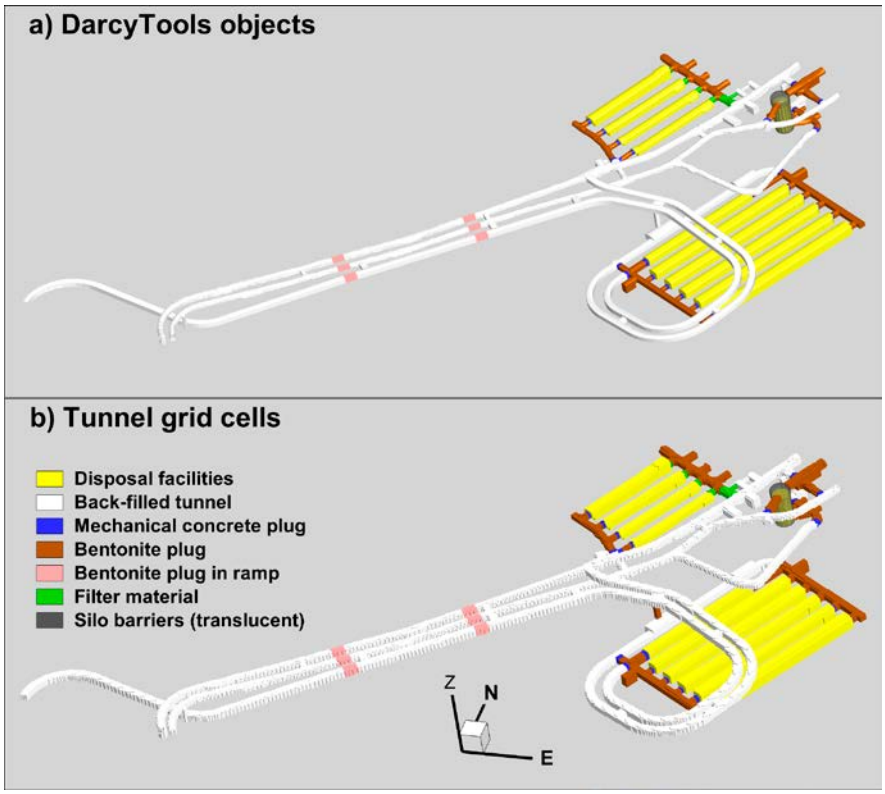

Figure 4-2. *DarcyTools objects used in discretisation of tunnel geometry.*

The planned SFR extension has a vertical ventilation shaft. By the time of the TD13 simulations, no decision had been taken concerning the potential needs to plug this shaft, and consequently there no such plug geometry data were available. In TD11 (Öhman et al. 2014) it was decided to assume the ventilation shaft to be bentonite-plugged from –88 to –120 m elevation (Figure 6-1b). This is implemented via the manually constructed DarcyTools object [R_Bentonite_in_L1BC_shaft_brown_pts.dat].

One part of the L1BC ramp is not "watertight" (L1BC_2DT_del3_white.stl). Gaps in the CAD object imply ambiguity in classification of cells by cell markers (e.g. in this case, a cluster of adjacent bedrock cells becomes erroneously classed as part of the L1BC ramp in the grid generation). This leakage was mended by inserting 4 triangles, after which the CAD data was converted into the DarcyTools object [R_2DT_del3_white.dat]. Even so, a single cell bedrock cell (centre coordinates 6706, 9950, –78, in the rotated model coordinate system) is still erroneously classed in the grid generation. This particular cell was therefore separately re-classed as bedrock, by introducing a "single point object" [R_BEDROCK_Fix_L1BC_2DT_del3_white.dat].

4.3 RLDM data

The RLDM data usage in the permafrost are the same as the ones used in TD11 (Öhman et al. 2014) and the temperate simulations thereof and related TD:s. Below only a summary of sections deemed essential is given.

4.3.1 Topography (DEM) and regolith layers

Modelled regolith layer geometry is delivered from the dynamic landscape model, RLDM (Brydsten and Strömgren 2013). Modelled regolith-layer data are defined in terms of upper-surface elevations and are delivered for the 6 selected time slices. The regolith layers are: 1) Quaternary deposits, 2) filling material, and 3) peat. Owing to a "fixed-bedrock" model convention used, the bedrock surface is modelled as static (i.e. envisaged as constant elevation over time). The bedrock surface can therefore be defined based on the original definition in the static regolith model.

Table 4-2. Regolith data files delivered from RLDM.

Filenames[1)]	Description	Usage
pdem<time slice>.asc pdem<time slice>.xyz	Upper peat surface elevation (m). Peat starts to form –500 AD. This layer is therefore missing in earlier time steps.	HSD parameterisation Point data used for basin filling, defining lake/river objects, grid generation
lpgd<time slice>.asc	The upper surface of lacustrine accumulation of postglacial deposits, elevation (m). Lacustrine accumulation begins 1500 AD. This layer is therefore missing in earlier time steps.	HSD parameterisation
mpgd<time slice>.asc	The upper surface of marine accumulation of post glacial deposits, elevation (m). The same layer is used from 7000 AD to 55,000 AD.	HSD parameterisation
gkl<time slice>.asc	The upper surface of glacial clay, elevation (m). The same layer is used from 7000 AD to 55,000 AD.	HSD parameterisation
fill<time slice>.asc	The upper surface of filling, elevation (m). This layer is used for all time steps.	HSD parameterisation
glfl<time slice>.asc	The upper glaciofluvial-material surface elevation (m). Thickness is constant during all time steps.	HSD parameterisation
till<time slice>.asc	The upper till surface elevation (m). Thickness is constant during all time steps.	HSD parameterisation
bedr<time slice>.asc bedr<time slice>.xyz	The upper bedrock surface, level in the height system RH 70 (m). The level has been corrected for all layers from –8000 AD to 55,000 AD using the Sea shoreline curve for the reference scenario.	HSD parameterisation Point data not used[2)]

[1)] Selected <time slice> are: 20,000 AD. Extensions *.asc are in GIS raster format, while *.xyz is in point-data ASCII format.

[2)] Owing to the “fixed-bedrock” convention used, the bedrock surface is modelled as static. The bedrock surface is therefore defined by the original definition in the static regolith model [bedrock_up_v2_2000AD.xyz], GIS #12_08.

The RLDM data have several different applications in modelling. The data are processed differently depending on application:

1) **Grid generation**: In the flow model, HSD is defined by grid cells between the bedrock surface (constant) and topography (varies over time, as modelled in RLDM). Grid generation requires pre-processing of geometrical data into so-called “DarcyTools objects” (constructed from *.xyz files).
2) **HSD parameterisation**: raster data (*.asc files, after fixed-bedrock conversion) are used directly in the model parameterisation.
3) **Visualisation**: visual confirmation of topography and surface hydrology objects, as well as, production of figures based on *.asc files converted into TecPlot *.plt format.

Model areas outside RLDM coverage are complemented by topography data from the static regolith model [DEM_xyz_batymetri_20120131.txt].

4.3.2 Processing RLDM data

The processing of RLDM data for input to the DarcyTools modelling is summarized in Table 4-3.

Table 4-3. RLDM data processing in 3 steps.

Purpose [input]	Execution code [output]
1. Conform to DarcyTools elevation reference system	
Convert regolith layer elevations (Table 4-2) into fixed-bedrock format. [*.asc], [*.xyz]	Future_HSD_data_to_fixed_Bedrock_format.f90 (adds suffix *“**_Fixed_bedrock**”) [*_Fixed_bedrock.asc], [*_Fixed_bedrock.xyz]
2. DarcyTools objects in grid generation	
Construct DarcyTools object defining topography and bedrock surface [pdem*_Fixed_bedrock.xyz] [bedrock_up_v2_2000AD.xyz]	DEM_to_DT_object.f (extensions *“.**dat**”, *“.**plt**”) [pdem*_Fixed_bedrock.dat], [pdem*_Fixed_bedrock.plt] [bedrock_up_v2_2000AD.dat], [bedrock_up_v2_2000AD.plt]
Rotate DarcyTools objects into local model coordinate system [pdem*_Fixed_bedrock.dat], [bedrock_up_v2_2000AD.dat]	Rotate_DT_objects.f90 (adds prefix “**R_**”*) [R_ pdem*_Fixed_bedrock.dat], [R_bedrock_up_v2_2000AD.dat]

4.3.3 Lakes

Lakes are used as prescribed head- and temperature boundary conditions in the flow model. More precisely, “Lake cells” are defined and refined in the computational grid by means of so-called “DarcyTools objects”. Lake cells are identified via a unique DarcyTools cell marker, which is translated into a prescribed-head value in the subsequent flow simulations. The prescribed-head values are taken from the modelled lake thresholds in RLDM. The number of lakes within the relevant flow model domain for 20,000 AD is only 2. Geometry of RLDM lakes and rivers are delivered in GIS vector format.

Implementation of geometrical data in the DarcyTools grid generation requires that data are converted into the so-called “DarcyTools object” file format. DarcyTools objects representing lakes, were created with the following 4 steps:

1. RLDM lake vector shapes are transformed into watertight 3D CAD volumes [*.stl], enclosing each lake water volume. The conversion is made in AutoCAD. The CAD objects are also translated from their original RT90 coordinate system by [–1626000.0, –6692000.0].
2. By means of the DarcyTools module OGN, CAD volumes are then converted into so-called “DarcyTools objects”. The conversion is a standard DarcyTools procedure.
3. Finally, lake objects are rotated into the local DarcyTools coordinate system by means of the Fortran code [Rotate_DT_objects.f90]. Pivot point in local coordinate system: [6400. 9200.], rotation angle: 32.58816946°.

These time-specific, individual lake objects are only used to define lake cells in the computational grid.

Additionally a set of lakes are delivered as output from a MikeShe simulation (Werner et al. 2013) These lakes (ponds and peatbogs) are defined from areas that become oversaturated in the MikeShe simulation with at least 0.5 metres of water. These ponds are used as a sensitivity case in the landscape scenarios used in the permafrost cases.

Implementation of geometrical data in the DarcyTools grid generation requires that data are converted into the so-called “DarcyTools object” file format. DarcyTools objects representing lakes, in the following 4 steps:

1. MIKE SHE lake vector shapes are transformed into watertight 3D CAD volumes [*.stl], enclosing each lake water volume. The conversion is made in AutoCAD. The CAD objects are also translated from their original RT90 coordinate system by [–1626000.0, –6692000.0].
2. By means of the DarcyTools module OGN, CAD volumes are then converted into so-called “DarcyTools objects”. The conversion is a standard DarcyTools procedure.
3. Finally, lake objects are rotated into the local DarcyTools coordinate system by means of the Fortran code [Rotate_DT_objects.f90]. Pivot point in local coordinate system: [6400. 9200.], rotation angle: 32.58816946°.

4.3.4 Rivers

Rivers are in two cases treated as prescribed temperature boundary conditions in the flow model. Geometry of RLDM lakes and rivers are delivered in GIS vector format.

Implementation of geometrical data in the DarcyTools grid generation requires that data are converted into the so-called “DarcyTools object” file format. DarcyTools objects representing lakes, in the following 4 steps:

1. River vector shapes are transformed into 2D CAD surfaces [*.stl]. The CAD objects are also translated from their original RT90 coordinate system by [–1626000.0, –6692000.0].
2. By means of the DarcyTools module OGN, CAD volumes are then converted into so-called “DarcyTools objects”. The conversion is a standard DarcyTools procedure.
3. Finally, river objects are rotated into the local DarcyTools coordinate system by means of the Fortran code [Rotate_DT_objects.f90]. Pivot point in local coordinate system: [6400. 9200.], rotation angle: 32.58816946°.

4.3.5 Relative sea level displacement in fixed-bedrock reference

In the fixed-bedrock reference system, shore-line retreat is modelled by means of relative sea level displacement (Table 4-4). The relative shore level data are taken from the Global warming climate case (SKB 2014c).

Table 4-4. Relative sea level at selected time slices.

Year AD	Relative sea level*, m
2000	–0.17
3000	–5.92
5000	–16.60
7000	–26.16
9000	–34.62
20,000	**–57.40**

* Land lift is expressed as a relative sea level displacement to the bedrock surface, since 1970 AD (reproduced from SKB 2014c).

5 Boundary conditions

5.1 Top boundary conditions

The top boundary conditions are basically the control of the model and results. It is readily seen in the results presented below that the assumptions of particularly the landscape control the results. This landscape evolution is uncertain in itself, but in permafrost simulations also concerning the aspect of limited information about, for instance, the behaviour of shallow ponds and peatbogs in the initial freezing process. It is thermally possible that these features may act as taliks for a significant period of time, as well as peat bogs often act as remaining permafrost patches during the melting of the permafrost.

The effect of different landscapes or surface systems is investigated by three different system scenarios. Figure 5-1 shows the landscape most exposed to open taliks. This landscape is created through a combination of water bodies created in a MIKE SHE simulation for an 11,000 AD DEM and the future lakes and rivers from the landscape evolution model (Brydsten and Strömgren 2013) of the 20,000 AD. All lakes are assigned elevation (head) based on the threshold value in the DEM and a positive bottom temperature of +4 Degrees C. Ponds are assigned elevation based on the MIKE SHE information of the water column thickness and a positive bottom temperature of +2 degrees C. The rivers follow the DEM surface and have a positive temperature of +2 degrees C. It is noted that the rivers are not specifically resolved in the grid generation and hence are represented with a width of the grid cells being 32 metres. This is indeed an over-estimation of river width during the permafrost periods simulated.

Figure 5-2 illustrates a case where all ponds and peatbogs are removed. The rivers still act as a positive temperature boundary of a width controlled by the grid cell size yielding an over-estimation of the river width. Figure 5-3 illustrates the most likely landscape scenario where ponds, peatbogs as well as rivers all are frozen and only the large enough lakes remain open and will act as taliks. The situation illustrated in Figure 5-2 and Figure 5-3 will in reality be more controlled by a regional groundwater gradient compared to the situation illustrated in Figure 5-1.

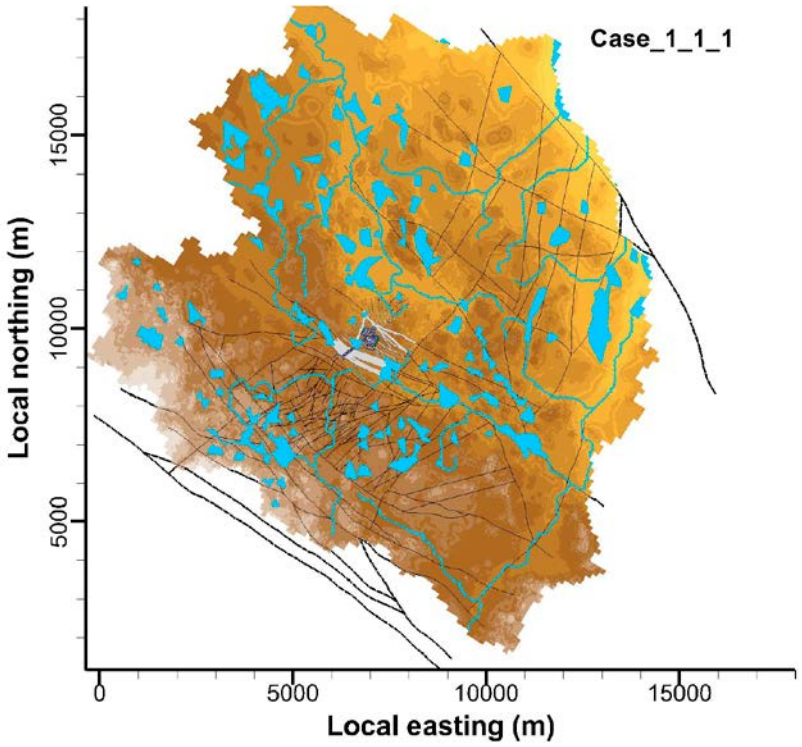

Figure 5-1. *Illustration of the top boundary conditions for a surface system with a high degree of exposure to open taliks.*

In a situation like the one illustrated in Figure 5-1 the regional gradient will be diminished in comparison to local gradients between different open taliks of different surface elevation. Figure 5-4 illustrates that a series of high elevation taliks from the situation illustrated in Figure 5-1 were kept open also in the scenarios with a landscape less exposed to taliks in order to mimic a super-regional gradient following the in general low and homogeneous surface topography gradient of Forsmark, Uppland.

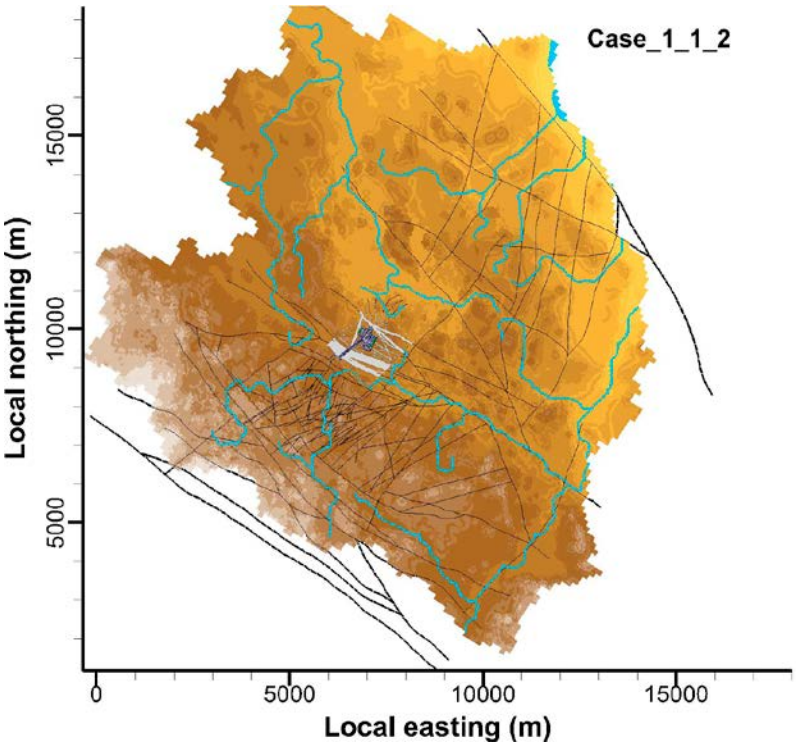

Figure 5-2. *Illustration of the top boundary conditions for a surface system with an intermediate degree of exposure to open taliks.*

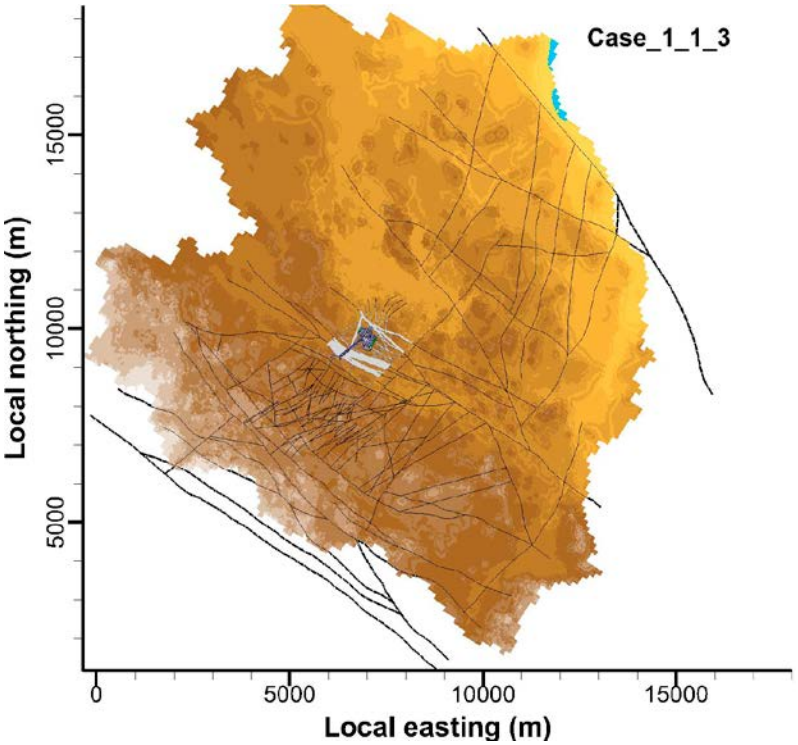

Figure 5-3. *Illustration of the top boundary conditions for a surface system with a low degree of exposure to open taliks.*

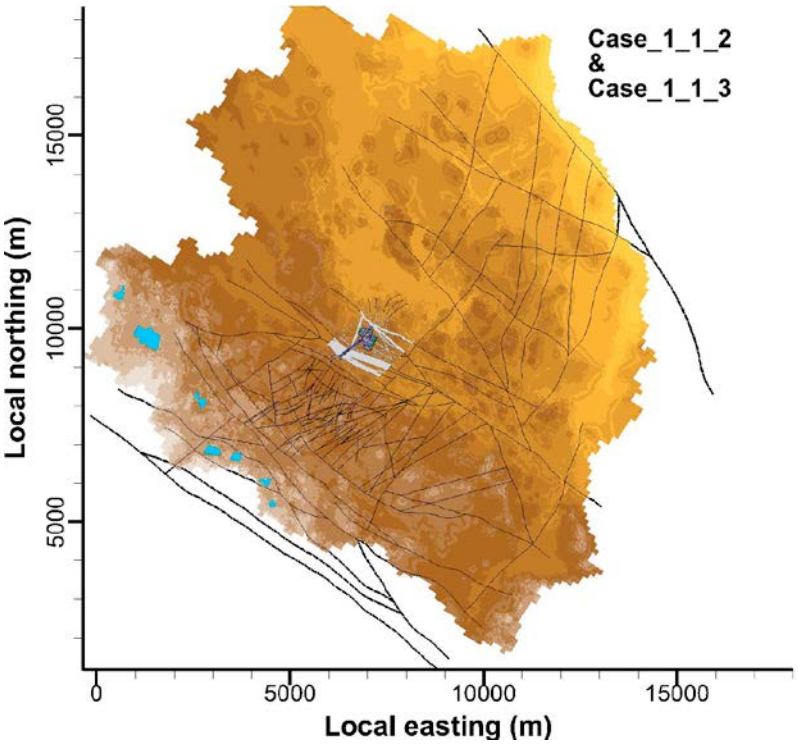

Figure 5-4. *Illustration of the top boundary conditions for a surface system. Illustrating the set of taliks used to mimic a super-regional groundwater gradient.*

5.2 Lateral and bottom boundaries

The lateral boundary conditions are no-flow boundaries for mass and heat, respectively. The bottom boundary is no-flow for mass, but for heat which has a specified heat flux of 0.034 W/m^2 (after Vidstrand et al. 2010).

6 Model parameterisation

The model parameterisation usage in the permafrost modelling is the same as the one used in the temperate modelling (Öhman et al. 2014). Below only a summary of sections deemed essential is given.

6.1 Tunnel parameterisation

The parameterisation of tunnel plugs and Silo barriers is taken from the intact plug case of (SKB 2014c) (see Table 6-1). General tunnel sections, ramps, and disposal facilities (except the Silo), which are not defined as plugs, are parameterised as back-fill with a conductivity of 10^{-5} m/s (Figure 6-1). The parameterisation is made via DarcyTools makers (referred to as Mk in Table 6-1), which define different tunnel sections. Special attention is given to the Silo, to ensure a realistic representation of the details in the parameterisation and particle-release locations (Figure 6-3).

Particle tracking performance measures address only the bedrock outside tunnel walls.

Table 6-1. Tunnel back-fill parameterisation (Figure 6-1 and Figure 6-3).

	Mk	Tunnel	Conductivity (m/s)	Description
SFR 1	11	1BTF	10^{-5}	Rock vaults, assumed to be backfilled by macadam. (Non-filled, open section of 1BLA not resolved.)
	12	2BTF		
	13	1BLA		
	14	1BMA		
	15/21[1)]	Silo interior	$5 \cdot 10^{-9}$	Outer concrete cylinder, inner vertical shafts with intervening concrete walls, waste packages and concrete grouting.
	16	1DT, 1BT	10^{-5}	Ramp backfilled with macadam.
	21[2)]	Silo exterior	10^{-5}	Compacted fill of friction material, e.g. crushed rock or macadam and, at the very top, with cement-stabilized sand.
			10^{-9}	Compacted fill of bentonite/sand mixture (10/90 percentage by weight) at the bottom and top of the silo.
			Single-layer walls: $K(z) = 2.1 \cdot 10^{-10} + 1.6 \cdot 10^{-12} * z$	Pure bentonite in silo walls, with hydraulic conductivity expressed as function of elevation, z (m RHB70), due to variable degree of self-compaction. In the lower part $K(z) \approx 9 \cdot 10^{-12}$ m/s and the upper part $K(z) \approx 9 \cdot 10^{-11}$ m/s.
SFR 3	22	2BLA	10^{-5}	Rock vaults, assumed to be backfilled by macadam. (Non-filled, open section of BLA caverns not resolved.)
	23	3BLA		
	24	4BLA		
	25	5BLA		
	26	2BMA		
	27	1BRT		
	28	1RTT	10^{-5}	Ramp backfilled with macadam.
Intact plugs	30	Blue	10^{-6}	Mechanical concrete plug (i.e. for mechanical support).
	31	Brown	10^{-10}	Hydraulic tight section with bentonite.
	32	Green	10^{-6}	Earth-dam plug, consisting of transition material (e.g. 30/70 bentonite crushed rock).
	33	Pink	$5 \cdot 10^{-10}$	Plugs in access tunnels, made up of 10 metre long tight hydraulic sections of bentonite surrounded by concrete plugs for mechanical support.

[1)] The silo is divided into two DarcyTools cell markers: particles are released from the inner concrete cylinder (Mk = 15), which is enclosed by barriers from which no particles are released (Mk = 21).

[2)] Conductivity parameterisation of the silo exterior not based on cell marking, but differentiated by geometrical bounds based on a combined interpretation of CAD data and SKB 2014c (see Figure 6-3).

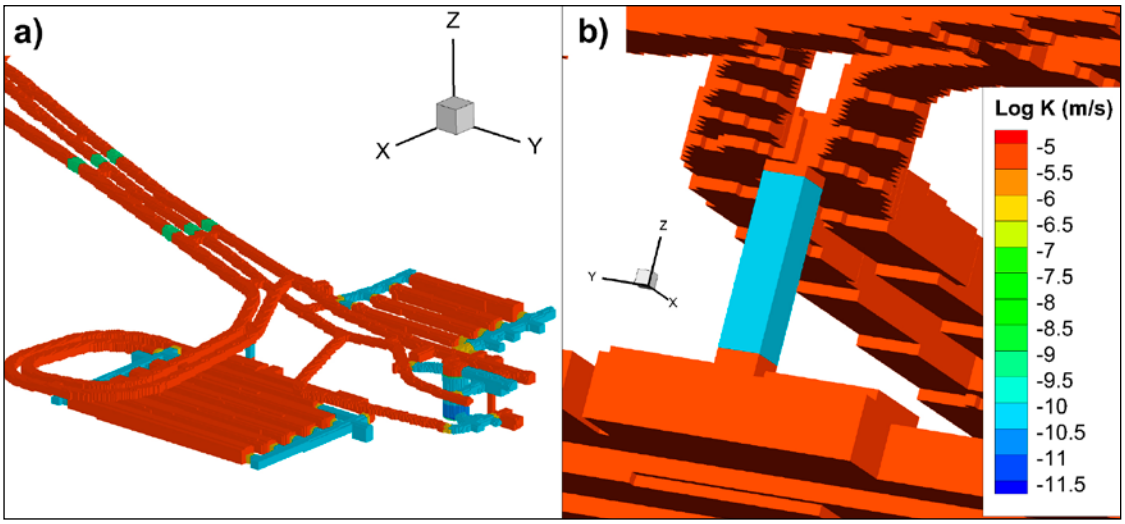

Figure 6-1. *Conductivity parameterisation of tunnel back-fill; a) existing SFR 1 and planned SFR extension, b) bentonite-filling in ventilation shaft assigned from –88 to –120 m elevation.*

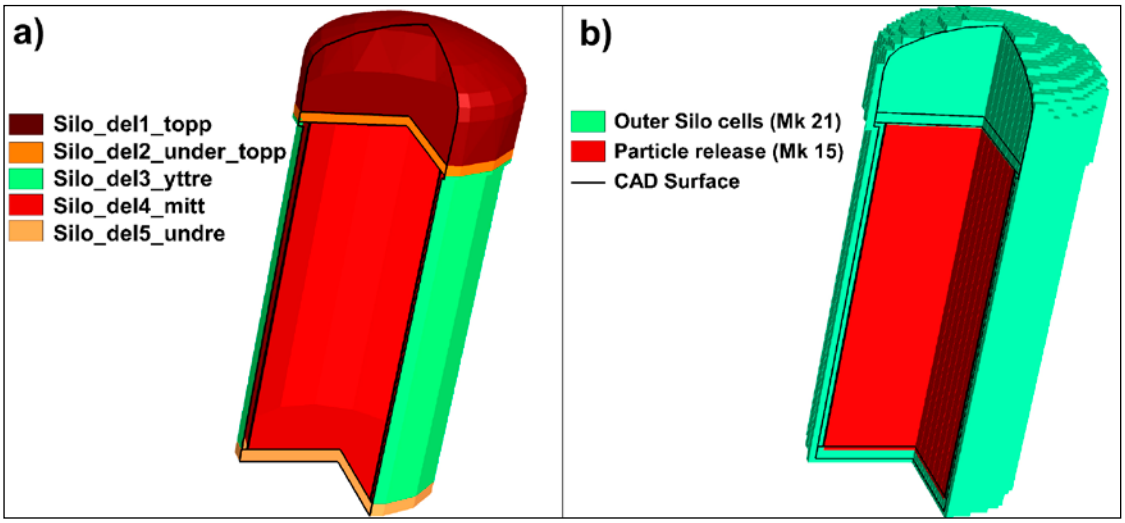

Figure 6-2. *Cell marking of the discretised Silo; a) Silo sub-volumes defined by CAD data (Table B-1), differentiated by colour, and b) defined particle-release location (CAD definitions in black lines).*

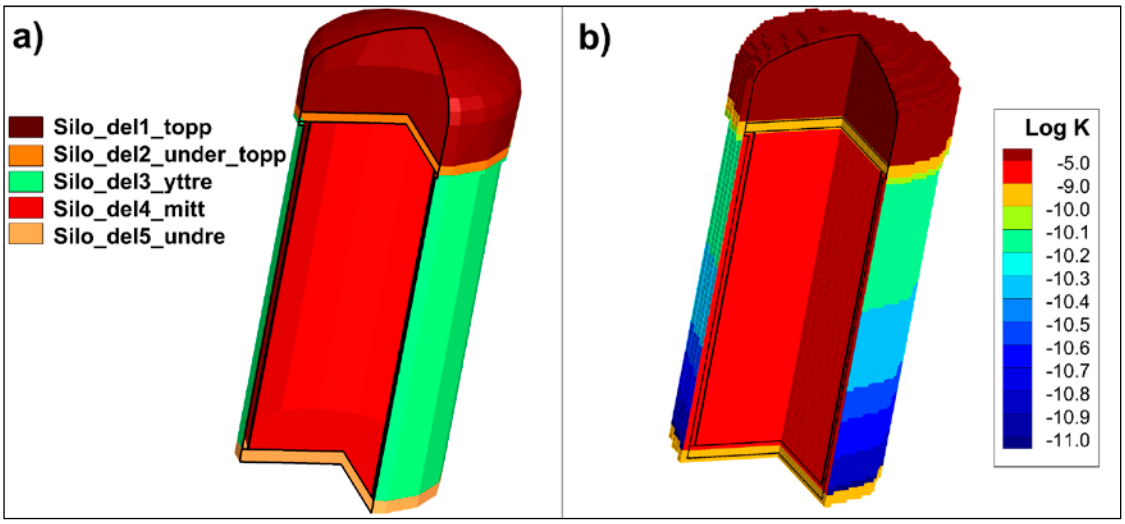

Figure 6-3. *Parameterisation of the Silo; a) Silo sub-volumes defined by CAD data (Table B-1), differentiated by colours, and b) assigned conductivity (CAD definitions in black lines).*

6.2 Bedrock cases inside SFR regional domain

The performance of the groundwater flow model is subject to conceptual uncertainty in the bedrock parameterization. In the permafrost simulations three bedrock cases are selected that are representative for covering the observed range of uncertainty in bedrock parameterisation. These three bedrock cases are selected based on flow through the eleven disposal facilities in SFR 1 and SFR 3:

1) One “low-flow” bedrock case (No. 15): bedrock parameterisation variant with low disposal-facility flows.
2) A base case: a basic model setup, representing “average bedrock characteristics” with median disposal-facility flows.
3) One “high-flow” bedrock case (No. 11): bedrock parameterisation variant with high disposal-facility flows.

Details of the different bedrock descriptions are found in the reporting of TD11.

Table 6-2. HRD realisations (Discrete fracture network + Unresolved PDZs).

Variant	Files	Description
R18	R_SFR_DFN_connected_R18_L1BC_knwn R_Unresolved_PDZ_R18_knwn	Optimistic realisation for existing SFR 1 (few large fractures connecting disposal facilities in existing SFR 1)
R85	R_SFR_DFN_connected_R85_L1BC_knwn R_Unresolved_PDZ_R85_knwn	Pessimistic realisation for existing SFR 1 (large fractures connecting disposal facilities in existing SFR 1)

6.3 Bedrock outside SFR regional domain

The bedrock description outside the SFR regional domain is taken from SR-Site/SDM-Site Forsmark and kept constant in all model setups.

Table 6-3. Fracture files used outside SFR regional domain.

Filename[1)]	Description	Source
PFM_zoner_med_hål_i_mitten	Parameterized HCD, outside SFR regional domain. Exclusion of HCD geometry inside SFR regional domain (+ entire ZFM871) described in Öhman (2010, Section 3.3.2). Converted from “dt” into “known-fracture format”.	861006_DZ_PFM_REG_v22_SJ.dt
UPDATED_SERCO_DFN_WITH_HOLE	Stochastic DFN outside SFR regional domain in “known-fracture format” (Figure 6-4). Original file from SDM-Site Forsmark, expanded to cover flow domain, as described in TD10 (SKBdoc 1395215).	SRS-FFM01-06_v4_alterFinal_nocpm_r1_sets1-65_all_96.asc EXTENDED_SERCO_DFN_WITH_HOLE
PLU_sheet_joints_truncated	Hydraulic deterministic structures (HCD), converted from ifz into “known-fracture format”, and locally reduced transmissivity near SFR ramp, as described in Öhman et al. (2013, Section 3.4.1).	081006_sheet_joints_v5.ifz
Parameterized_SFR_BRIDGES	Used to fill in geometrical discontinuities when merging SFR HCDs with those in SDM-Site Forsmark. Parameterised and converted from xml into “known-fracture format” via RVSinfo.	SKBdoc 1282650 – SFR DZ MASTER v1.0-bridges.xml (internal document)

[1)] All fracture files are rotated into the local model coordinate system. The prefix “R_” is added to all rotated files, denoting the rotated coordinate system.

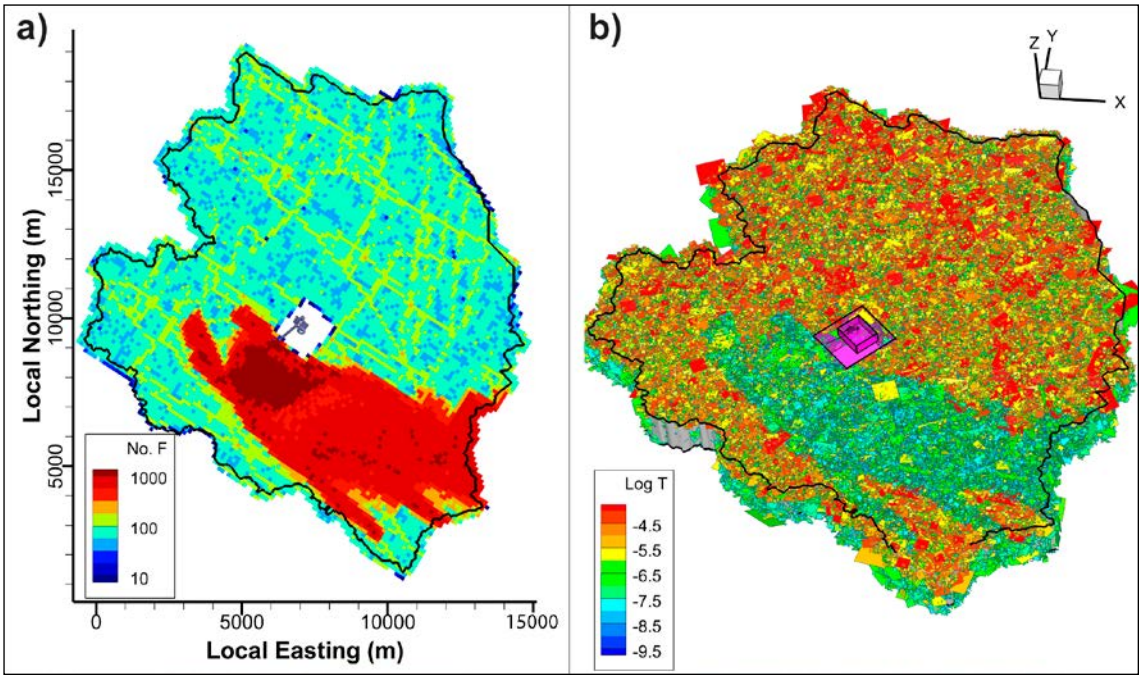

Figure 6-4. *HRD outside SFR regional domain, defined by [UPDATED_SERCO_DFN_WITH_HOLE]; a) fracture-count map and b) 3D visualisation of fracture planes (cf Figure 4-1).*

6.4 HSD parameterisation

HSD conductivity of RLDM regolith layers are based on Table 2-3 in Bosson et al. (2010). Porosity is assumed equal to specific yield (Table 6-4). However, particle-tracking performance measures address only bedrock properties and therefore porosity and FWS are nullified in the particle tracking to eliminate the risk of contribution to accumulated transit time or F-quotient.

Table 6-4. HSD hydraulic conductivity of regolith layers.

Regolith layer	K_h (m/s)	K_v (m/s)	Porosity[4] (–)	Layer definition (Table 4-2)
Peat[1]	3.00E–7	3.00E–7	0.2	From <lpgd> to <Filled_pdem[1]>
Lacustrine accumulation of postglacial deposits	1.50E–8	1.50E–8	0.05	From <mpgd> to <lpgd>
Marine accumulation of post glacial deposits	1.50E–8	1.50E–8	0.03	From <gkl> to <mpgd>
Glacial clay	1.50E–8	1.50E–8	0.03	From <fill> to <gkl>
Filling[2]	1.50E–4	1.50E–4	0.2	From <glfl> to <fill>. Special handling of the SFR pier[2].
Glaciofluvial material	1.50E–4	1.50E–4	0.2	From <till> to <glfl>
Till	7.50E–6	7.50E–7	0.05	From <bedr> to <till>
Upper bedrock[3]	≥ 3.0E–8	≥3.0E–8	≥1.0E–5	Thin soil coverage (soil depth < 4.0 m) and elevated bedrock (z > –10 m)

[1] Note that the upper surface of peat refers to the basin-filled DEM (Section 4.3.2), which implies that local basins are assumed to be peat-filled, or at least filled with a relatively high-conductive material.

[2] Special attention is given to the SFR pier. To avoid artefacts in the determination of the surface head in the Pier, the "conductivity of fill" is expanded 2 grid cells, horizontally (2×8 m). Below an elevation of z = –3 m, a layer of till is assumed to underlie the filled areas around the SFR pier [prpgen_TD11_Model_parameterisation.f].

[3] A minimum bedrock conductivity of $3 \cdot 10^{-8}$ m/s is assigned in two cases: 1) at thin soil coverage (soil depth < 4 m), and above an elevation of –10 m (this is to compensate that DFN coverage above z = 0 m, is unavailable outside the SFR regional domain, Section 6.3).

[4] HSD porosity set equal to 0.0 in particle tracking to avoid unintentional contribution to performance measures of the bedrock.

6.5 Thermal properties

The values used in the flow simulations are shown in Table 6-5. The properties assigned are based on estimated mean values taken from Hartikainen et al. (2010) and Sundberg et al. (2009).

Table 6-5. Thermal properties.

Property	Intact Rock	Deformation zone	Till	Gravel	Fill	Clay	Peat
Thermal conductivity [W/mK]	3.45	2.9	2.1	2.9	2.9	1.0	0.6
Heat capacity [J/m^{3}K]	$2.2 \cdot 10^6$	$2.7 \cdot 10^6$	$2.5 \cdot 10^6$	$2.7 \cdot 10^6$	$2.7 \cdot 10^6$	$3.4 \cdot 10^6$	$4.2 \cdot 10^6$

6.6 State laws

Under temperate conditions and within the depth interval in which the SFR facility is located, state laws could be viewed as independent of temperature. However, for periglacial climate condition much flow occurs at temperatures close to 0°C, so this independence of temperature does not apply.

In the simulations the state laws governing density and viscosity have been made dependent on temperature and specified to fit the observations for the temperature interval between 0 and 20°C (see Chapter 3 Concepts and methodology).

The freezing and associated phase change of water is accounted for within the DarcyTools solver. The freezing temperature is fixed to 0°C independent of pressure and salinity. The shallow location of the SFR facility and the fact that glacial conditions are not modelled means that these limitations in the modelling are justified. The freezing/thawing interval used in the DarcyTools freezing routine is specified to occur over one degree, primarily adjusted to yield as good an approximation as possible to the situation likely to apply in the general bedrock.

7 Simulation sequence

7.1 Grid generation

Computational grids are generated by means of the DarcyTools module GridGen. The grids are unstructured, which allows the flexibility of local refinement (e.g. near ground surface and tunnel geometry). The discretization is carried out via a sequence of commands specified in the standardised Compact Input File on xml-format, [cif.xml] (Svensson et al. 2010). A discretisation command consists of a geometrical reference (i.e. DarcyTools objects in Chapter 3) and either: 1) a specification of local maximum cell side length, and/or 2) classification of grid subdomains by means of a cell marker ID. Cell-marker IDs have a key role in subsequent modelling; for example they are used in property assignment, boundary conditions, and particle release points.

7.2 ECPM up-scaling

DarcyTools employs a Continuum Porous-Medium (CPM) representation (Svensson et al. 2010), in which the hydraulic properties of a flowing fracture network are approximated by those of a porous medium. DarcyTools allows transferring fracture-network characteristics onto its computational grid by means of geometric up-scaling. The up-scaled properties are referred to as Equivalent Continuum Porous Medium (ECPM) properties. As the ECPM approach is based on an underlying DFN model, the resulting ECPM properties are a reflection of the fracture network. Geometric up-scaling does not always ensure hydraulic consistency between the complex heterogeneity of the underlying flowing fracture network and the approximated ECPM. However, the finer the grid cell resolution the better the reflection of the underlying fracture network.

DarcyTools employs a staggered grid arrangement with ECPM properties which are derived from geometric fracture-network up-scaling over local control volumes (Svensson et al. 2010). This staggered grid involves scalar properties, defined at cell centres (e.g. porosity and flow-wetted surface area), and so-called tensor properties, stored at cell walls (e.g. conductivity). In other words, scalar and tensor ECPM properties do not represent identical control volumes, but are offset by half a grid cell.

A consequence of the staggered grid arrangement is that each step in the cell-jump particle tracking approach involves one cross-cell flow, but two grid-cell porosities and FWS-values The ECPM conversion relies on several approximations:

- All fractures inside a cell-wall control volume contribute to advection.
- The advection takes place over their full fracture surface area.
- Porosity of fractures below the fracture-size truncation is negligible.

Kinematic porosity is a critical parameter for determining particle transport time. Unfortunately the parameter is difficult to measure in field. In the numerical flow model, kinematic porosity can be calculated in the GEHYCO algorithm (Svensson et al. 2010) by the ECPM conversion of transport apertures of fracture networks. Äspö Task Force 6C results (Dershowitz et al. 2003), suggested a fracture transport aperture correlated to transmissivity, according to

$$e_t = 0.46\sqrt{T} \qquad (7\text{-}1)$$

which was also used as a starting point for model calibration in SDM-Site Forsmark (Follin 2008). For SR-PSU, it has been decided to up-scale porosity (i.e. an ECPM property) from the transport apertures of the underlying fracture network, as defined by Eq. 7-1, with a minimum porosity value set to 10^{-5} [–].

ECPM up-scaling is featured by the DarcyTools module FracGen (GEHYCO algorithm) (Svensson et al. 2010), for which all input data are specified in a standardised Compact Input File, on xml-format [cif.xml].

7.3 Flow simulations

Flow simulations are coupled via a staggered process that is the sweep loop, available within the DarcyTools solver. The simulations are run without a specified storativity which implyies steady-state simulations and in the case of DarcyTools also a fixed porosity. The simulations are transient with respect to heat transport and the simulations represent the heat solution after a specified time. This time was chosen in order to reach a pre-defined depth of the 0-degree isotherm.

7.4 Post process

Post-processing of flow solutions is conducted by means of the DarcyTools module PropGen, as compiled from customized Fortran codes. The post-processing is executed in batches, in which the traceability between input and output data is automatized. Two types of performance measures are analysed:

1) Flows in disposal facilities.
2) Bedrock retention properties, by means of particle tracking.

7.4.1 Flow-field analysis

The flow-field post processing is done in order to calculate cross flow over disposal facilities as a performance measure.

Cross flow refers to the total flow over a predefined cross-sectional area in the computational grid. This area is the interface between a sub-unit of interest, i, (e.g. a tunnel section or bedrock surface) and surrounding, arbitrary grid cells, j. For example, this ij-interface may refer to a tunnel wall between tunnel cells identified by marking, Mk = i and surrounding bedrock/plugs with grid-cell marking Mk = $j \neq i$ (i.e. j may include several cell markers).

7.4.2 Particle tracking

In DarcyTools, particles are tracked in a deterministic way by being moved along a discretised path within the local finite-element velocity-field. The particle tracking routine in DarcyTools, PARTRACK, has two modes of operation (Svensson et al. 2010).; the first is the classic way of moving the particle along the local velocity vector, whereas the second method uses the so called "flux-weighting" approach, and works as follows.

- A particle entering a scalar cell will, if no dispersion effects are activated, stay in the cell for a time that is equal to the free volume of the cell divided by the flow rate through the cell.
- When the particle is ready to leave the cell, it will leave through one of the cell walls that has an outgoing flow direction. The choice between cell walls with an outgoing flow is made with a likelihood that is proportional to the outflows. If several particles are traced, the cloud will thus split up in proportion to the flow rates. Complete mixing in a cell is assumed.

Three performance measures are calculated:

- Flow path length L [L]
- Advective travel time t_w [T]
- Flow-related transport resistance F [TL^{-1}]

Unfortunately, the inbuilt particle-tracking methods are not very feasible due to the extensive demands of SR-PSU (involving multiple model setups and large numbers of particles released). Instead, particle tracking is performed as a post process applied to a steady-state flow field (i.e. outside the DarcyTools flow solver). There are reasons for using a standalone post processing:

1) Rapid execution time (processing steady-state solutions reduces particle tracking to a geometric problem, circumventing the computational demanding (and time consuming!) iterative time-stepping within the DarcyTools solver. The post-processor algorithm also allows simultaneous processing in parallel working folders)

2) Flexibility: the code can easily be adapted to meet the various needs within the SR-PSU project (customize definition of performance measures, target specific issues, etc.)

3) File management: Output can be customized to meet the particular demands within the SR-PSU project (e.g. applying file-naming conventions, condense output to reduce file sizes, export in defined delivery structures, user-specified Tecplot output, etc.)

The used algorithm [P_track_random_TD11_deplete_loops.f] is based on the cell-jump method, where particles (i.e. discretisation of water volumes) traverse the computational grid on a cell-to-cell basis, according to inter-nodal flow between cells. The method assumes complete mixing of water in all cells, which implies a stochastic component in the routing of particle trajectories.

A particle trajectory represents the advective flow path of a discretised water volume through the bedrock. The purpose of particle tracking is to quantify cumulative bedrock retention properties along an ensemble of trajectories. The evaluation targets only the retention properties in bedrock, and therefore no properties of tunnel-backfill or HSD are included in the performance measures.

Particles are released uniformly within disposal facilities (identification via cell markers). However, the "release point" is defined as the tunnel-wall passage (i.e. or put in other words, the bedrock entry point). Proportionality exists between density of particle-release points and tunnel-wall flow in terms of a bounding envelope. Particle trajectories are terminated at the bedrock surface, where the "exit point" is defined by the cell wall between a bedrock cell and a HSD cell.

The probability, P_{ij}, of navigating from cell i to cell j is assumed to be proportional to the flow in that direction, Q_{ij}, where a *sign-criterion* applies to Q_{ij}, depending on the *direction* of particle tracking:

$$P_{ij} = \frac{Q_{ij}}{\sum Q_{ij}} \tag{7-2}$$

Particle tracking can be performed in two directions: in *forward* tracking, only outward-directed flows are included in Eq. 7-2, whereas in *backward* tracking only includes inward-directed flows.

The total path length of particle trajectories, L_r (m), is calculated as the sum of distances between the centre points of passed cell walls. Note that cell-wall centre coordinates are used in the path-length calculation, as opposed to cell-centre coordinates. The purpose of using cell-wall centre coordinates is to allow for diagonal "corner cutting" through cells (i.e. to some extent reducing the overestimation due to rectilinear nature of particle jumps).

Likewise, the advective travel time of a flow path, $t_{w,r}$ (y), is determined as the sum of travel times for each discrete particle step along the trajectory. The discrete travel time, t_{ij}, taken to move from the centre of cell i to the centre of cell j, is assumed to be:

$$t_{ij} = \frac{n_i V_i + n_j V_j}{2Q_{ij}} \tag{7-3}$$

where n is cell porosity and V is cell volume (i.e. the product nV is the cell volumetric water content). The factor 2 in the denominator reflects that only *half* of the cell volumetric water contents, $n_i V_i$ and $n_j V_j$, are involved in the inter-nodal flow Q_{ij}.

Analogously, the cumulative flow-related transport resistance, F_r (y/m), or F-quotient, is also determined as the summed bedrock properties for discrete particle jumps. The transport resistance for each discrete jump, from cell centre i to cell centre j, F_{ij}, is assumed to be:

$$F_{ij} = a_w t = \frac{fws_i + fws_j}{2Q_{ij}} \tag{7-4}$$

where a_w is flow-wetted surface area per volume of water and *fws* is the flow-wetted surface areas in cells i and j, respectively (based on Svensson et al. (2010) and MARFA interface). Calculated performance measures only reflect the bedrock; therefore both porosity and *fws* are nullified in tunnel backfill and in overlying sediments.

8 Results

8.1 Flow-related transport resistance

Particles are released, according to earlier descriptions, within the three rock vaults, 1BMA, the Silo, and 2BMA which were chosen since they puts bounds to the possible release locations. The particles are thereafter tracked in a forward direction until each of the individual particles reach the interface between the bedrock and the soil domain (HSD).

Figure 8-1 to Figure 8-3 below show cumulative distribution (probability) plots of the discharge flow-related transport resistance for all the released particles divided into release from different rock vaults. Figure 8-1 illustrates the results for a release in a landscape affected by shallow permafrost; with a 0-degree isotherm at approximately –60 metres elevation additionally the landscape is assumed with a high degree of taliks. Taliks are assumed in all peat filled depressions and small ponds within the model domain along with the, at the future time 20,000 AD,future streams and lakes. In this relatively exposed landscape the fluxes at the SFR facility is for some of the rock vaults higher than the temperate conditions of a similar shoreline situation. The calculated flow-related transport resistance is found higher than $1 \cdot 10^3$ y/m; the rock vault belonging to the SFR 1 exhibit a median value around $2 \cdot 10^4$ y/m while the rock vault belonging to SFR 3 is found around $1 \cdot 10^5$ y/m. The calculated values of releases from the Silo shows the largest spread which is a result due to both large depth difference in release locations and also due to the mostly low permeable bedrock surrounding the Silo.

Figure 8-2 and Figure 8-3 illustrates the difference between shallow permafrost and a somewhat deeper case where the 0-degree isotherm has reached a depth below all rock vaults of SFR 1 (approximately to a depth of –90 metres elevation). Both cases are calculated with a landscape only exposed to discharge taliks in the far away located lakes that is valid for the time 20,000 AD. This landscape is deemed more realistic compared to the more talik exposed cases that produces higher flows and hence is incorporated as sensitivity cases since the forecast of landscape and climate evolution are uncertain. The calculated flow-related transport resistance is found higher than $1 \cdot 10^4$ y/m; the rock vaults belonging to the SFR 1 and SFR 3 exhibits a median value around $2 \cdot 10^5$ y/m. The calculated values of releases from the three release locations show similar spread and also the difference between shallow permafrost and deeper is minor. This is since the change in hydraulic properties around SFR 1 is still small due to the assigned interval within with the bedrock change from unfrozen to completely frozen is minor and hence that all three release locations experience an almost horizontal flow with most released particles discharging in the two far away lake taliks.

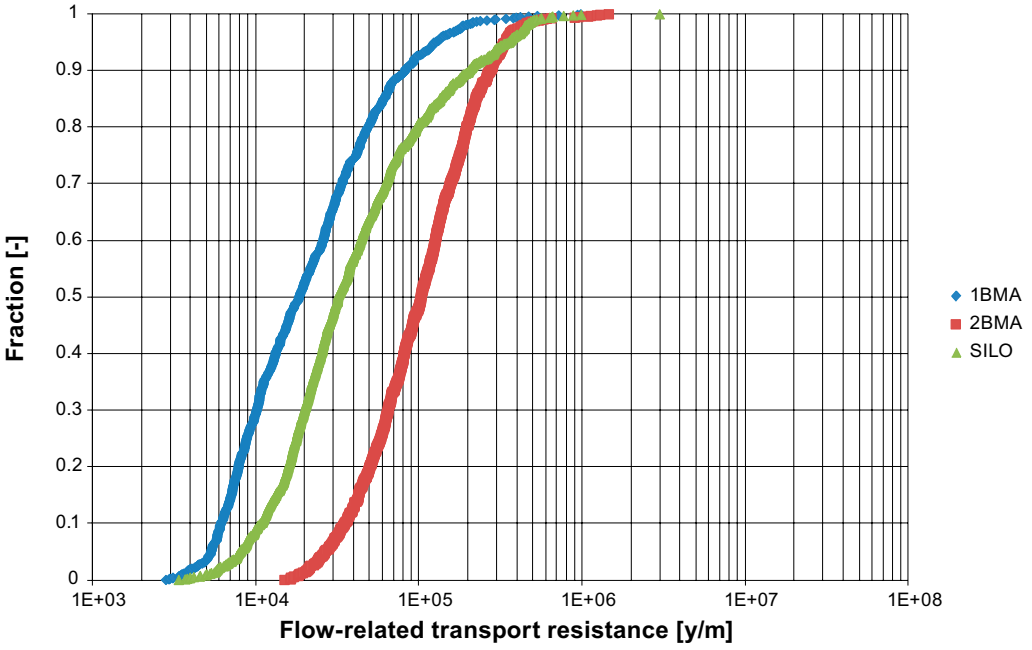

Figure 8-1. *Illustration of flow-related transport resistance results for Case_1_1_1 (see Table 2-4).*

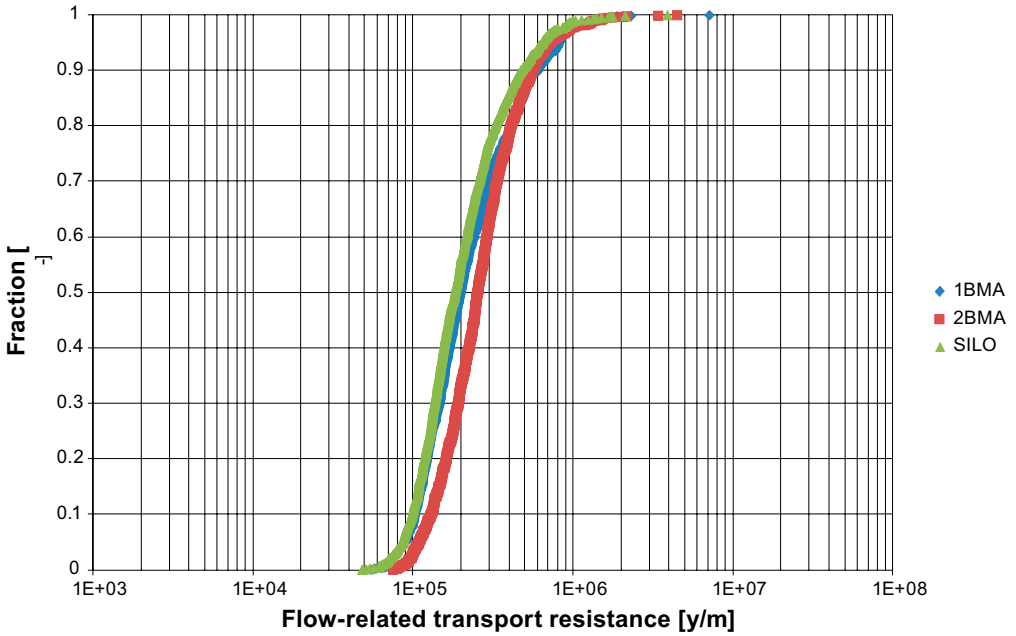

Figure 8-2. *Illustration of flow-related transport resistance results for Case_1_1_3 (see Table 2-4).*

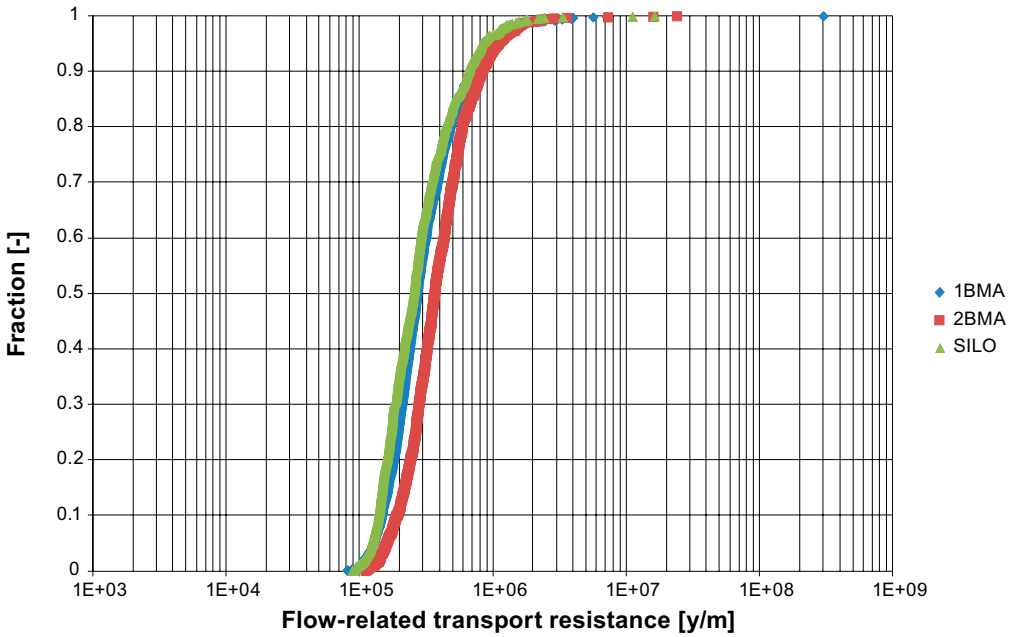

Figure 8-3. *Illustration of flow-related transport resistance results for Case_1_3_3 (see Table 2-4).*

8.2 Cross-Flow (Q)

The total inflow (and outflow) to all the rock vaults in SFR 1 and SFR 3 has been calculated in each simulation.

Figure 8-4 illustrates the difference between two different types of top boundary conditions. In permafrost simulations herein the top boundary condition is set as a specified pressure boundary condition with atmospheric pressure at ground surface. The idea behind this assumption is that during the cold and dry conditions of permafrost, enough water is still available to maintain a groundwater table or, more correctly stated, saturated conditions at ground surface exists at all times. However, under temperate conditions the permeability of the ground may not be the limiting factor determining the recharge. Hence in this type of environment the specified pressure top boundary condition set at ground surface may locally induce the effect of small hills and depressions. The BaseCase Hybrid

results illustrated in Figure 8-4 are taken from the temperate simulations reported in Öhman et al. (2014), the BaseCase Pressure results are the results from the permafrost models without a frozen ground condition, that is similar as a temperate condition. In the comparison of results of total flow the BaseCase Hybrid is used. This top boundary is explained in Chapter 4.

The simplification of the top boundary condition in groundwater flow simulations of periglacial climate condition is primarily done due to numerical reasons. But the assumption of a groundwater table at the ground surface has been identified and validated by different investigations. Bosson et al. (2012) investigated the periglacial influence on the hydrology and concluded that even cold and dry climate, preferential during permafrost conditions, could create a hydrological system containing more groundwater than during temperate systems. Person et al. (2007) concluded that the unfrozen water content under permafrost conditions is sufficient to maintain the groundwater table at or close to the surface.

Figure 8-5 illustrates the results of shallow permafrost but different landscape descriptions. In the results it is noteworthy that the lowest total flows is exhibit in a landscape with less open taliks, these flows are primary controlled by a regional groundwater gradient imposed in the model with a series of open locations in the upstream part of the model domain. Secondly it is significant that in a case with many open taliks sitting close or even on-top of the SFR facility the total flow through some of the rock vaults are increased as compared to temperate conditions. This is especially significant for the SFR 3 facility that for all comparative cases show an increase in total flow.

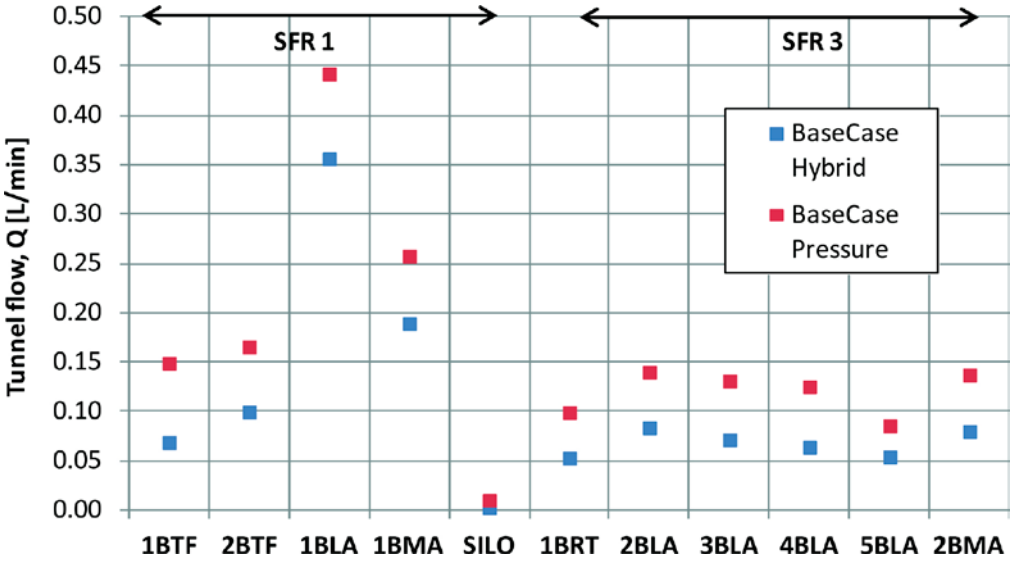

Figure 8-4. *Comparison of resulting cross flows for two types of top boundary conditions.*

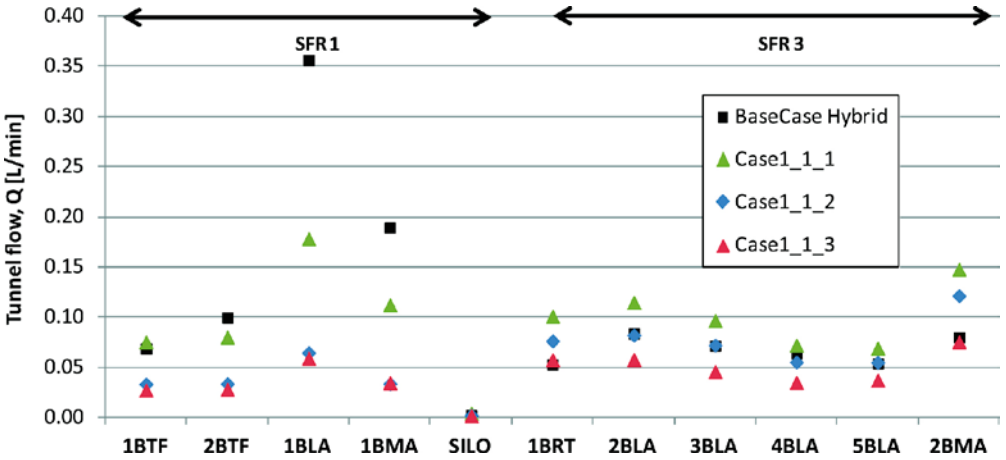

Figure 8-5. *Cross flows for different surface systems and shallow permafrost (see Table 2-4 for case description).*

In Figure 8-6 the difference between shallow permafrost and deeper permafrost reaching down into the SFR 1 rock vaults is shown. Most rock vaults indicate that the total flow will decrease with deeper permafrost also in a case with many open taliks. However, in the SFR 3 facility the effect is less and the 2BMA rock vault actually indicate a minor increase in total flow with deeper permafrost.

Figure 8-7 illustrates similar as Figure 8-5 the effect of different landscape scenarios. However, Figure 8-7 shows the results of deep permafrost reaching beneath the SFR 1 rock vaults. In Figure 8-7 the results are significant for concluding that deeper permafrost lower the total flow. The effect in SFR 1 is clear but again the results in the much deeper SFR 3 are less conclusive.

Figure 8-8 illustrates the results of a singular case of deep permafrost and compares the three different bedrock cases identified as the base case (Case 1) and the high and low extreme (Case 11 and 15). On the scale presented here the 2BMA rock vault is the most sensitive to different bedrock settings. And it is clear that differences in bedrock characteristics are as important as the depth of the permafrost as long as the frozen ground is primarily above the rock vaults.

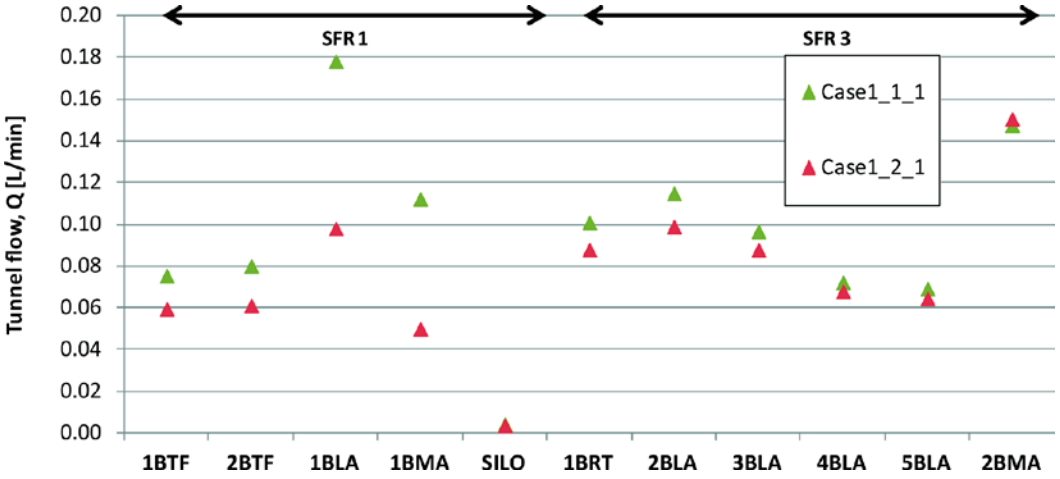

Figure 8-6. *Cross flows comparison between deeper and shallow permafrost for a highly exposed surface system as of open taliks (see Table 2-4 for case description).*

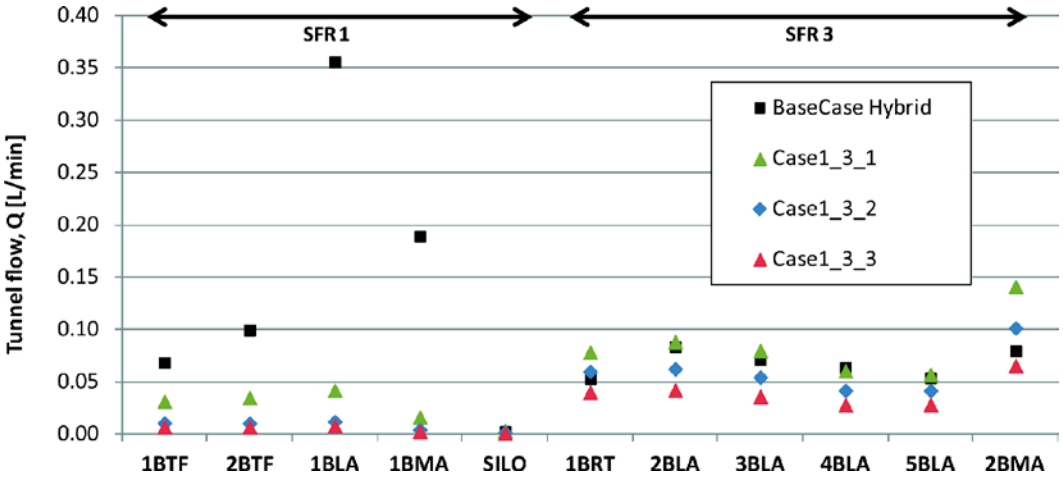

Figure 8-7. *Cross flows for different surface systems and deeper permafrost (see Table 2-4 for case description).*

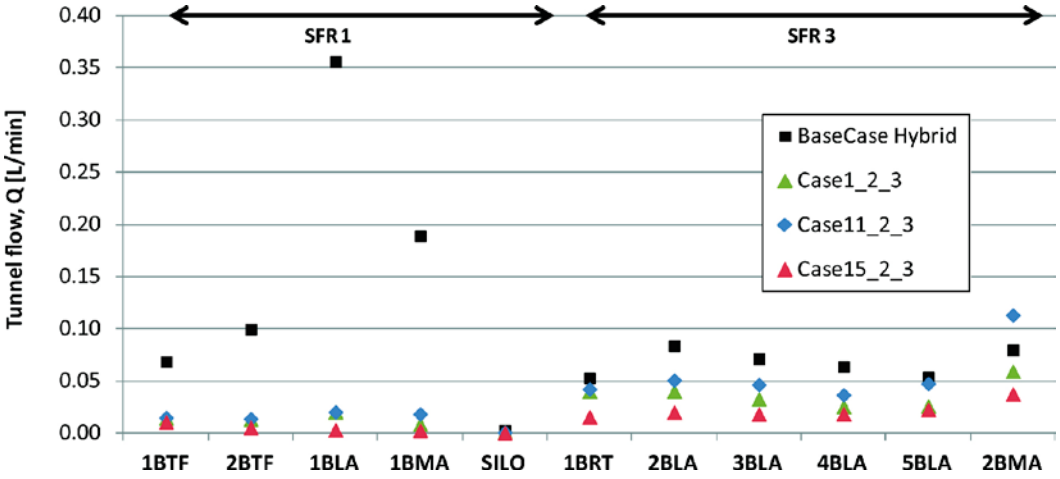

Figure 8-8. *Cross flows for a surface system of least exposure to open taliks and deeper permafrost reaching within SFR 1 rock vaults). Comparison of different bedrock cases (see Table 2-4 for case description).*

8.3 Tunnel wall specific flow

Particles are released at the tunnel wall in 1,000 locations of identified outflow within the three rock vaults, 1BMA, the Silo, and 2BMA. The same locations are used for all particle tracking. The particles are thereafter tracked in a forward direction until each of the individual particles reach the interface between the bedrock and the soil domain (HSD).

Figure 8-9 to Figure 8-11 below show cumulative distribution (probability) plots of the discharge specific flow at the starting locations for the particles released. The plots are for all the released particles divided into release from different rock vaults.

Figure 8-9 illustrates very similar behavior or velocity profiles between the rock vaults in SFR 1 and SFR 3. The Silo flows are however significantly lower. Compared to the cases illustrated in Figure 8-10 and Figure 8-11 with significant less exposure to taliks in the landscape the results in Figure 8-9 shows a larger spread with both smaller flows as well as larger specific flows at certain locations.

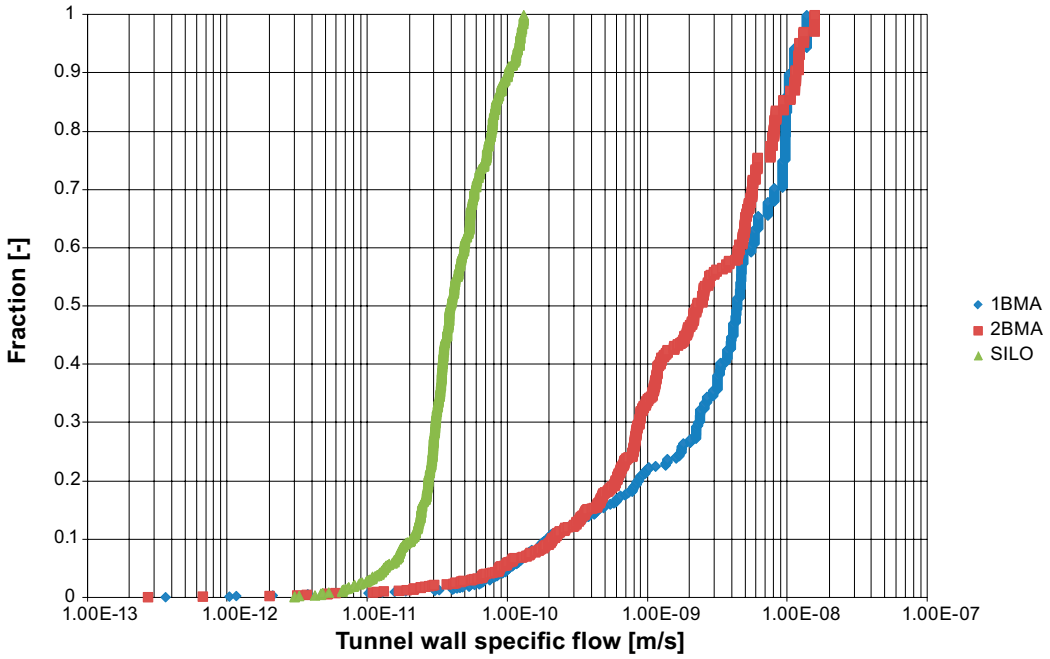

Figure 8-9. *Illustration of tunnel wall specific flow results for Case_1_1_1 (see Table 2-4).*

Differences between the shallow permafrost and the deeper permafrost cases are most clearly seen for specific flows at the tunnel walls in SFR 1 that are significantly shifted towards lower values. This result is illustrated in Figure 8-10 and Figure 8-11.

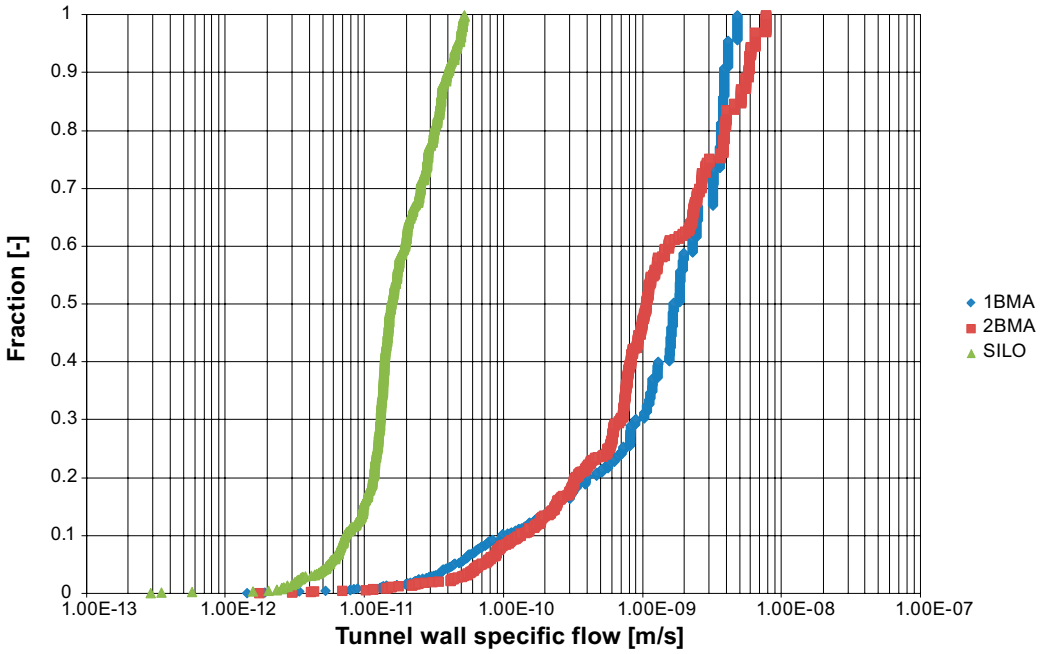

Figure 8-10. *Illustration of tunnel wall specific flow results for Case_1_1_3 (see Table 2-4).*

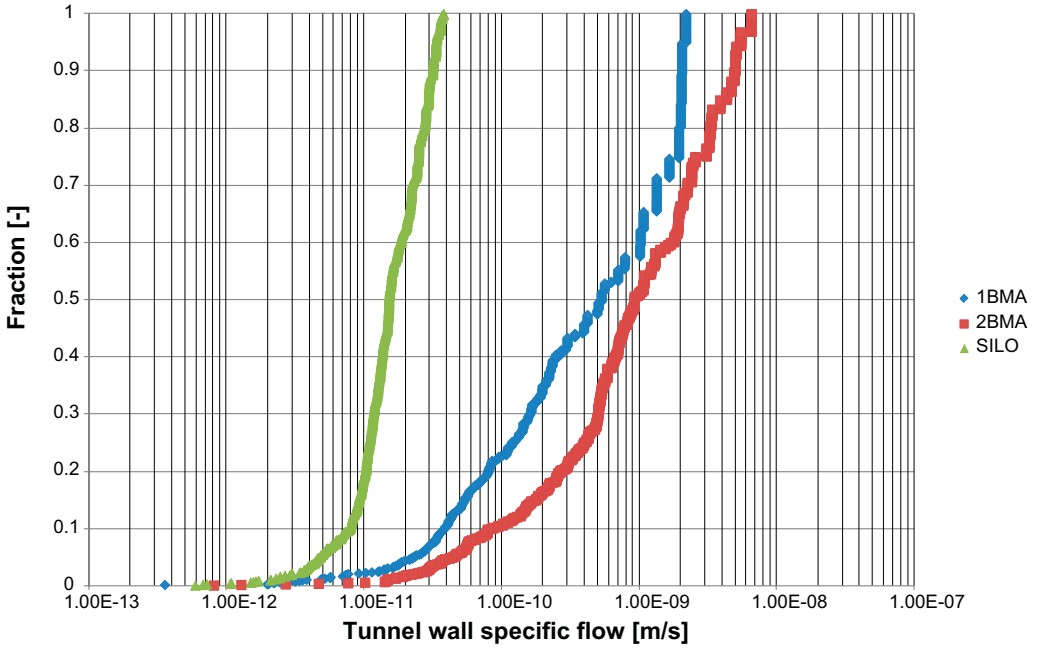

Figure 8-11. *Illustration of tunnel wall specific flow results for Case_1_3_3 (see Table 2-4).*

8.4 Exit locations

The SFR facility contains ten rock vaults and a Silo. Particles are released at the tunnel wall in 1,000 locations of identified outflow within the three rock vaults, 1BMA, the Silo, and 2BMA. The same locations are used for all particle tracking. The particles are thereafter tracked in a forward direction until each of the individual particles reach the interface between the bedrock and the soil domain (HSD). It is noted that all the conditions are fixed during the particle tracking, which is a simplification since the boundary conditions at ground surface change continuously during temperate, periglacial, as well as during glacial conditions.

The exit locations are predominantly found well within the physical boundaries of the model domain and, as a matter of fact, mostly within the lake taliks in the domain as seen in Figure 8-12. In Figure 8-12, more than 99% of the particles discharge in the taliks, whereas some particles discharge through the permafrost layer. That is, the permafrost has a low permeability (bedrock permeability is at maximum reduced five orders of magnitude), but it is not impervious. It could also be noted that the exit locations in the permafrost is governed by the deformation zones.

Figure 8-12 illustrates the shallow permafrost with few taliks and a regional groundwater gradient from southwest towards northeast. In contrast exit locations from a shallow permafrost case with many open taliks are illustrated in Figure 8-13. In this model the largest taliks, the lake taliks in northeast has no influence at all. Instead the system is totally controlled by local ponds and peat bogs being assigned talik conditions along with the rivers being active in the near-region of the SFR facility. The differences between the different landscape conditions concerning top boundary conditions are described in Chapter 4.

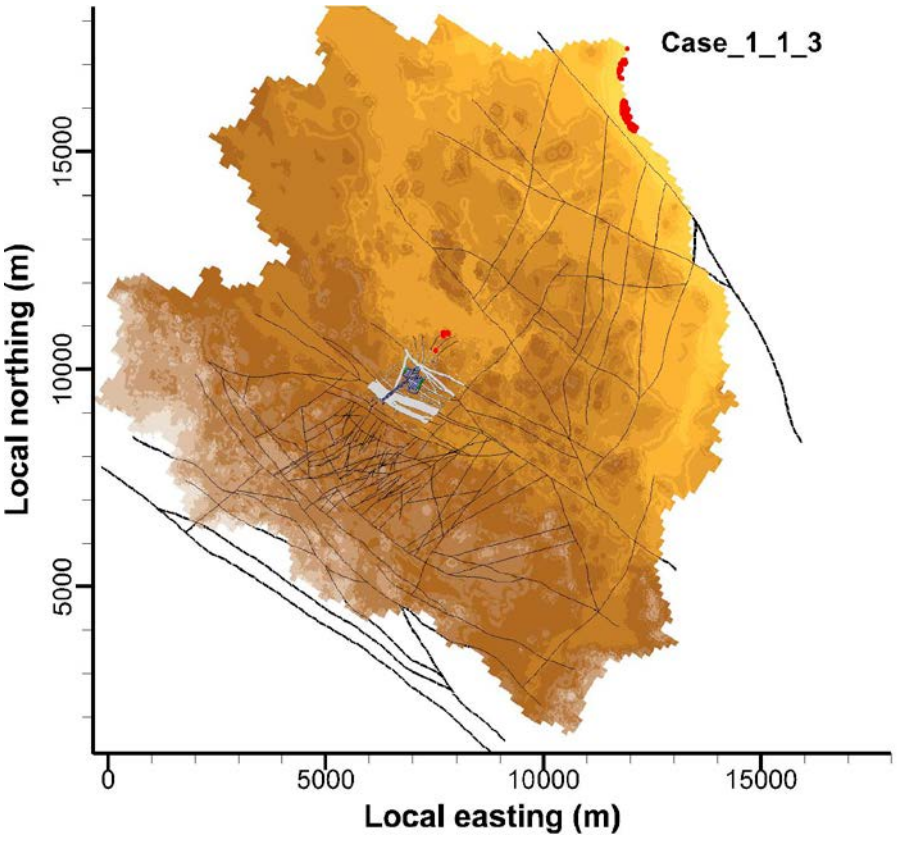

Figure 8-12. *Illustration of exit locations for a shallow permafrost and the least exposure to open taliks (Case_1_1_3) (see Table 2-4 for case description).*

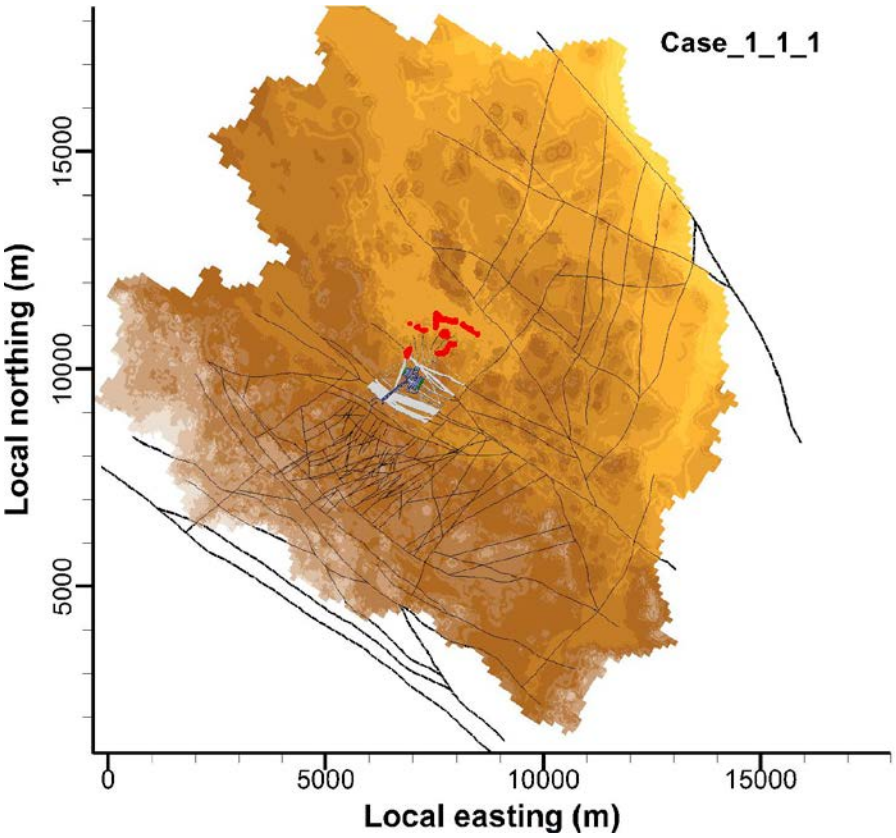

Figure 8-13. *Illustration of exit locations for a shallow permafrost and high exposure to open taliks (Case_1_1_1)) (see Table 2-4 for case description).*

8.5 Transit time (advective travel time)

Particles are released at the tunnel wall in 1,000 locations of identified outflow within the three rock vaults, 1BMA, the Silo, and 2BMA. The same locations are used for all particle tracking. The particles are thereafter tracked in a forward direction until each of the individual particles reach the interface between the bedrock and the soil domain (HSD).

Figure 8-14 to Figure 8-16 below show cumulative distribution (probability) plots of the discharge travel times for all the released particles divided into release from different rock vaults. Figure 8-14 illustrates the results for a release in a landscape affected by shallow permafrost. The case is characterised by a 0-degree isotherm at approximately –60 metres elevation; in addition, the landscape is assumed to have a high degree of taliks. Taliks are assumed in all peat filled depressions and small ponds within the model domain along with the, at the future time 20,000 AD, future streams and lakes. In this relatively exposed landscape the fluxes at the SFR facility is for some of the rock vaults higher than the temperate conditions of a similar shoreline situation. The calculated travel times are longer than 0.5 year; the rock vault belonging to the SFR 1 exhibits a median value around 2 years while the rock vault belonging to SFR 3 is found to have a median travel time of around 10 years. The calculated values of releases from the Silo show the largest spread, but with a median value around 3 years. The large spread is a result due to both large depth difference in release locations and also due to the mostly low permeable bedrock surrounding the Silo.

Figure 8-15 and Figure 8-16 illustrate the difference between shallow permafrost and a somewhat deeper case where the 0-degree isotherm has reached a depth below all rock vaults of SFR 1 (approximately to a depth of –90 metres elevation). Both cases are calculated with a landscape only exposed to discharge taliks in the far away located lakes; this situation is valid for the time 20,000 AD. This landscape is deemed more realistic compared to the more talik exposed cases that produce higher flows and hence is incorporated as sensitivity cases since the forecast of landscape

and climate evolution are uncertain. The calculated travel times are longer than 20 years; the rock vaults belonging to the SFR 1 and SFR 3 exhibit a median value around 60 years. The calculated values of releases from the three release locations show similar spread and also the difference between shallow permafrost and deeper is minor. This is since the change in hydraulic properties around SFR 1 is still small due to the assigned interval within which the bedrock change from unfrozen to completely frozen and hence all three release locations experience an almost horizontal flow with most released particles discharging in the two far away lake taliks.

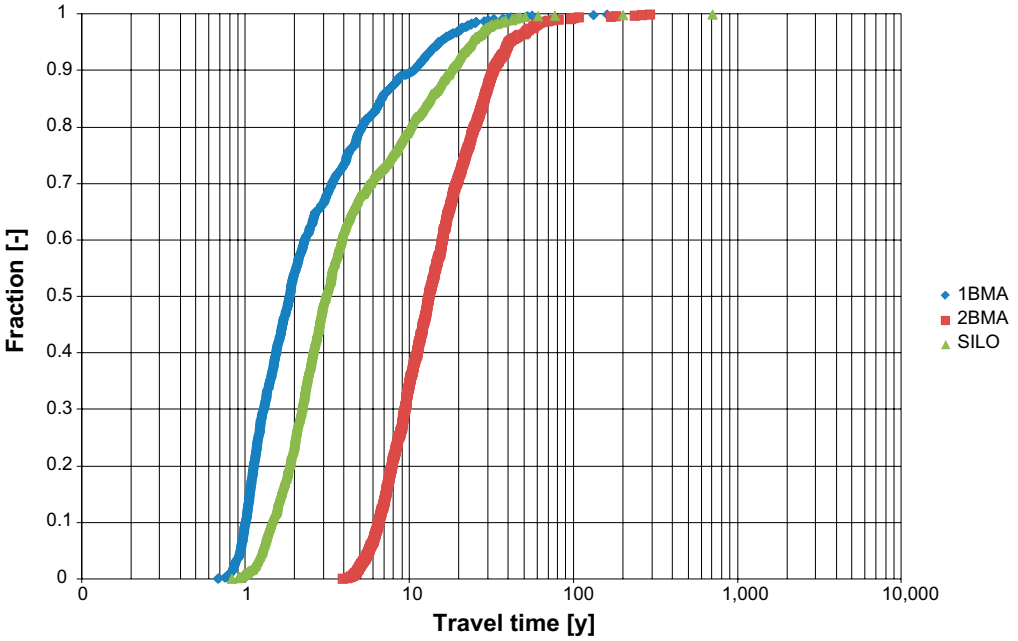

Figure 8-14. *Illustration of advective travel time results for Case_1_1_1) (see Table 2-4 for case description).*

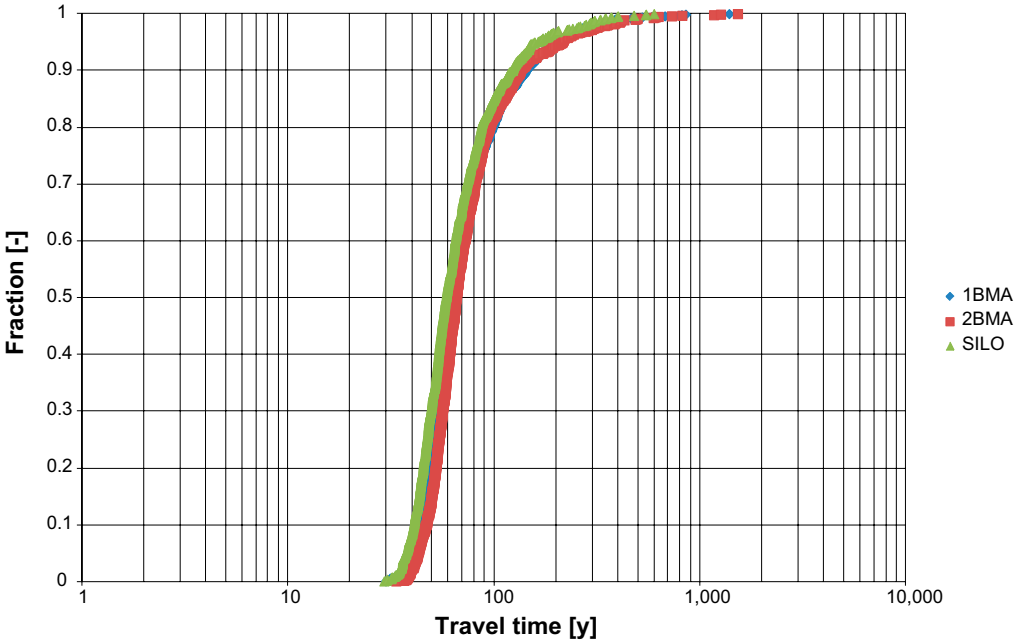

Figure 8-15. *Illustration of advective travel time results for Case_1_1_3 (see Table 2-4 for case description).*

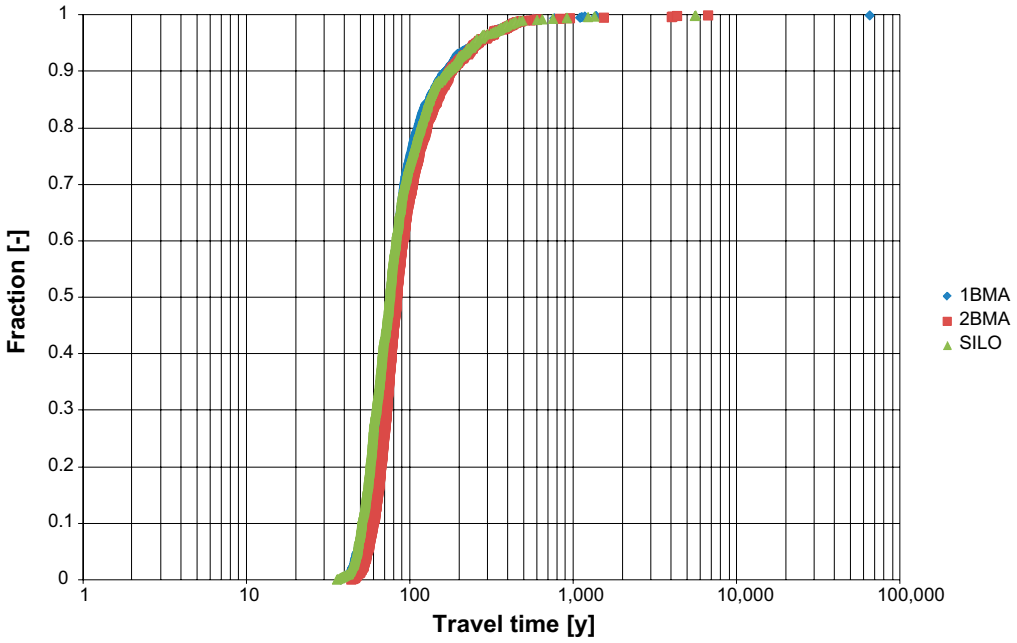

Figure 8-16. *Illustration of advective travel time results for Case_1_3_3 (see Table 2-4 for case description).*

8.6 Path length

Particles are released at the tunnel wall in 1,000 locations of identified outflow within the three rock vaults, 1BMA, the Silo, and 2BMA. The same locations are used for all particle tracking. The particles are thereafter tracked in a forward direction until each of the individual particles reach the interface between the bedrock and the soil domain (HSD).

Figure 8-17 to Figure 8-19 below show cumulative distribution (probability) plots of the discharge path lengths for all the released particles divided into release from different rock vaults. Figure 8-17 illustrates the results for a release in a landscape affected by shallow permafrost. The case is characterised by a 0-degree isotherm at approximately –60 metres elevation; in addition, the landscape is assumed to have a high degree of taliks. Taliks are assumed in all peat filled depressions and small ponds within the model domain along with the, at the future time 20,000 AD, future streams and lakes. In this relatively exposed landscape the fluxes at the SFR facility is for some of the rock vaults higher than the temperate conditions of a similar shoreline situation. The calculated path lengths are found longer than 400 metres; the rock vault belonging to the SFR 1 exhibit a median value around 600 metres while the rock vault belonging to SFR 3 is found to have a median path length of around 2,000 metres.

The particles traveling from SFR 1 and the Silo exhibit a slight shift in the distribution plot at about 90% and 70% respectively. This shift is also apparent for the Silo in the less exposed landscape cases illustrated in Figure 8-18 and Figure 8-19. The shift is primarily related to that some particles take a somewhat deeper route towards the discharge. In the analysed models this effect is over-exaggerated due to the omission of saline waters at depth.

Figure 8-18 and Figure 8-19 illustrate the difference between shallow permafrost and a somewhat deeper case where the 0-degree isotherm has reached a depth below all rock vaults of SFR 1 (approximately to a depth of –90 metres elevation). Both cases are calculated with a landscape only exposed to discharge taliks in the far away located lakes; this situation is valid for the time 20,000 AD. This landscape is deemed more realistic compared to the more talik exposed cases that produce higher flows and hence are incorporated as sensitivity cases since the forecast of landscape and climate evolution are uncertain. The calculated path lengths are found longer than 200 metres; the rock vaults belonging to the SFR 1 and SFR 3 exhibit a median value around 10,000 metres.

The calculated values of releases from the three release locations show similar spread and also the difference between shallow permafrost and deeper is minor, except for a slightly smaller amount of particles from SFR 1 escaping through the permafrost in the deeper permafrost case. The minor difference is since the change in hydraulic properties around SFR 1 is still small due to the assigned interval within which the bedrock change from unfrozen to completely frozen and hence all three release locations experience an almost horizontal flow with most released particles discharging in the two far away lake taliks.

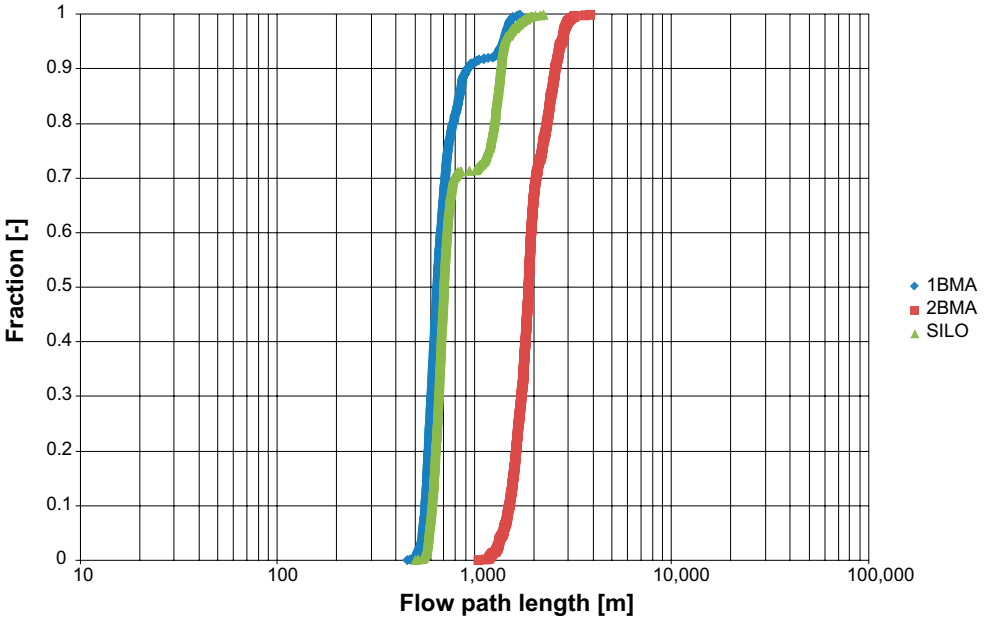

Figure 8-17. *Illustration of path length results for Case_1_1_1 (see Table 2-4 for case description).*

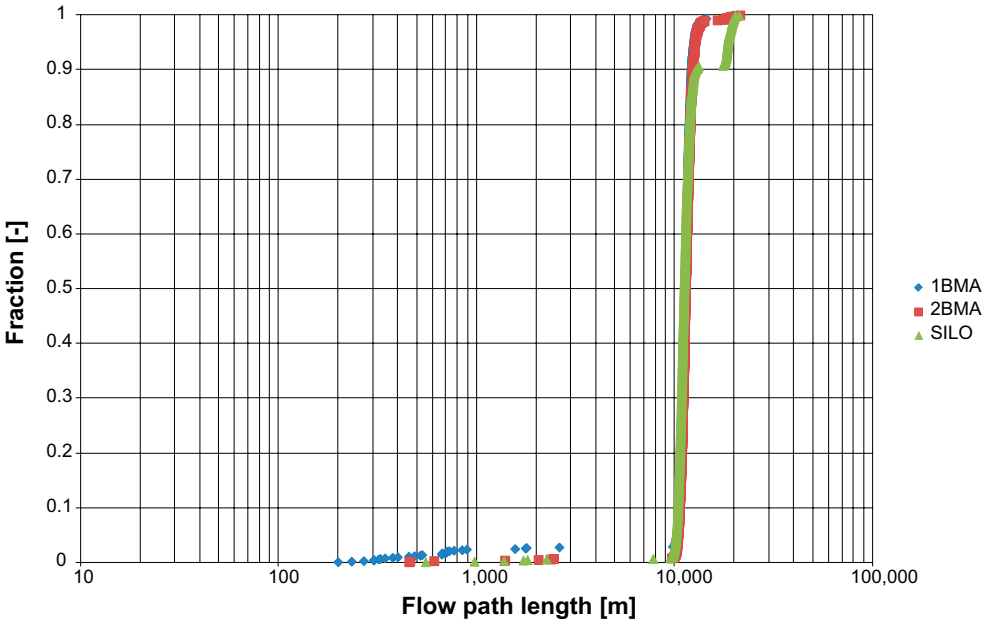

Figure 8-18. *Illustration of path length results for Case_1_1_3 (see Table 2-4 for case description).*

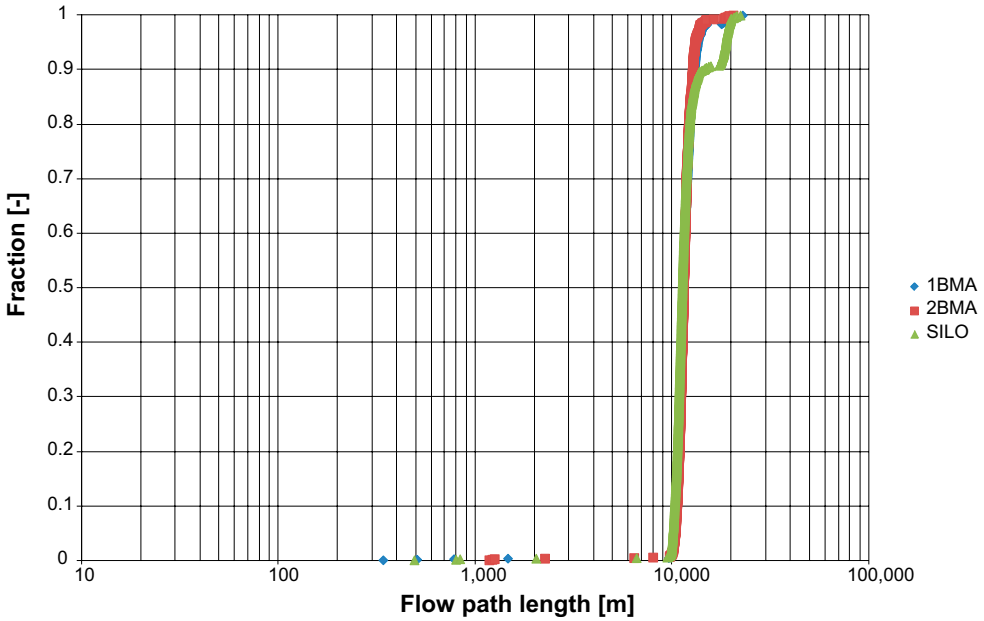

Figure 8-19. *Illustration of path length results for Case_1_3_3 (see Table 2-4 for case description).*

9 Conclusions

Main conclusions from the study of the period with periglacial climate conditions are:

- During periglacial climate conditions the most relevant scenarios for the Forsmark area reduce the total flow through the rock vaults and significantly increases the path lengths, travel times and flow-related transport resistance values. However, the climate conditions are uncertain and dependent on the extension and amount of taliks in the flow domain; some of the rock vaults may experience some small increases in total flows.
- Concerning resulting uncertainty in total flows, the underlying uncertainty in climate conditions is not larger than the underlying uncertainty stemming from the different bedrock cases. The exit locations and flow-related transport properties are not significantly effected by the uncertainty in bedrock properties. However, for all scenarios the exit locations are controlled by the predefined talik locations.

References

SKB's (Svensk Kärnbränslehantering AB) publications can be found at www.skb.se/publications. References to SKB's unpublished documents are listed separately at the end of the reference list. Unpublished documents will be submitted upon request to document@skb.se.

Bense V F, Person M A, 2008. Transient hydrodynamics within intercratonic sedimentary basins during glacial cycles. Journal of Geophysical Research 113, F04005. doi:10.1029/2007JF000969

Bosson E, Sassner M, Sabel U, Gustafsson L-G, 2010. Modelling of present and future hydrology and solute transport at Forsmark. SR-Site Biosphere. SKB R-10-02, Svensk Kärnbränslehantering AB.

Bosson E, Sabel U, Gustafsson L-G, Sassner M, Destouni G, 2012. Influences of shifts in climate, landscape, and permafrost on terrestrial hydrology. Journal of Geophysical Research 117, D05120. doi:10.1029/2011JD016429

Boulton G S, Slot T, Blessing K, Glasbergen P, Leijnse T, van Gijssel K, 1993. Deep circulation of groundwater in overpressured subglacial aquifers and it's geological consequences. Quaternary Science Reviews 12, 739–745.

Brydsten L, Strömgren M, 2013. Landscape development in the Forsmark area from the past into the future (8500 BC–40,000 AD). SKB R-13-27, Svensk Kärnbränslehantering AB.

Burt T P, Williams P J, 1976. Hydraulic conductivity in frozen soils. Earth Surface Processes 1, 349–360.

Dershowitz W, Winberg A, Hermanson J, Byegård J, Tullborg E-L, Andersson P, Mazurek M, 2003. Äspö Hard Rock Laboratory. Äspö Task Force on modelling of groundwater flow and transport of solutes. Task 6c. A semi-synthetic model of block scale conductive structures at the Äspö HRL. SKB IPR-03-13, Svensk Kärnbränslehantering AB.

Follin S, 2008. Bedrock hydrogeology Forsmark. Site descriptive modelling, SDM-Site Forsmark. SKB R-08-95, Svensk Kärnbränslehantering AB.

French H M, 1996. The periglacial environment. 2nd ed. Harlow: Longman.

Gascoyne M, 2000. A review of published literature on the effects of permafrost on the hydrogeochemistry of bedrock. Posiva 2000-09, Posiva Oy, Finland.

Haldorsen S, Heim M, 1999. An Arctic groundwater system and its dependence upon climate change: an example from Svalberg. Permafrost and Periglacial Processes 10, 137–149.

Hartikainen J, Kouhia R, Wallroth T, 2010. Permafrost simulations at Forsmark using a numerical 2D thermo-hydro-chemical model. SKB TR-09-17, Svensk Kärnbränslehantering AB.

Johansson E, Berglund S, Lindborg T, Petrone J, van As D, Gustafsson L-G, Näslund J-O, Laudon H, 2014. Hydrological and meteorological investigations in a periglacial lake catchment near Kangerlussuaq, west Greenland – presentation of a new multi-parameter dataset, Earth System Science data.

Joyce S, Simpson T, Hartley L, Applegate D, Hoek J, Jackson P, Swan D, Marsic N, Follin S, 2010. Groundwater flow modelling of periods with temperate climate conditions – Forsmark. SKB R-09-20, Svensk Kärnbränslehantering AB.

Kane D L, Stein J, 1983. Water movement into seasonally frozen soils. Water Resources Research 19, 1547–1557.

Kleinberg R L, Griffin D D, 2005. NMR measurements of permafrost: unfrozen water assay, pore-scale distribution of ice, and hydraulic permeability of sediments. Cold Regions Science and Technology 42, 63–77.

Lemieux J-M, Sudicky E A, Peltier W R, Tarasov L, 2008a. Simulating the impact of glaciations on continental groundwater flow systems: 1. Relevant processes and model formulation. Journal of Geophysical Research 113, F03017. doi:10.1029/2007JF000928

Lemieux J-M, Sudicky E A, Peltier W R, Tarasov L, 2008b. Simulating the impact of glaciations on continental groundwater flow systems: 2. Model application to the Wisconsinian glaciation over the Canadian landscape. Journal of Geophysical Research 113, F03018. doi:10.1029/2007JF000929

Lemieux J-M, Sudicky E A, Peltier W R, Tarasov L, 2008c. Dynamics of groundwater recharge and seepage over the Canadian landscape during the Wisconsinian glaciation. Journal of Geophysical Research 113, F01011. doi:10.1029/2007JF000838

Maxe L, 2003. Bestämning av markmaterialets specifika yta: resultat från svenska sand-, grus-, morän- och lerprofiler. Rapport, Institutionen för Mark- och Vattenteknik, KTH. (In Swedish.)

McEwen T, de Marsily G, 1991. The potential significance of permafrost to the behaviour of a deep radioactive waste repository. SKI Report 91:8, Statens kärnkraftinspekton (Swedish Nuclear Power Inspectorate).

Odén M, Follin S, Öhman J, Vidstrand P, 2014. SR-PSU Bedrock hydrogeology. Groundwater flow modelling methodology, setup and results. SKB R-13-25, Svensk Kärnbränslehantering AB.

Person M, McIntosh J, Bense V, Remenda V H, 2007. Pleistocene hydrology of North America: the role of ice sheets in reorganizing groundwater flow systems. Reviews of Geophysics 45, RG3007. doi:10.1029/2006RG000206

Rhén I, Follin S, Hermanson J, 2003. Hydrological Site Descriptive Model – a strategy for its development during site investigations. SKB R-03-08, Svensk Kärnbränslehantering AB.

SKB, 2013. Site description of the SFR area at Forsmark at completion of the site investigation phase, SDM-PSU Forsmark. SKB TR-11-04, Svensk Kärnbränslehantering AB.

SKB, 2014a. Safety analysis for SFR. Long-term safety. Main report for the safety assessment SR-PSU. TR-14-01, Svensk Kärnbränslehantering AB.

SKB, 2014b. Climate and climate related issues for the safety assessment SR-PSU. SKB TR-13-05, Svensk Kärnbränslehantering AB.

SKB, 2014c. Input data report for the safety assessment SR-PSU. SKB TR-14-12, Svensk Kärnbränslehantering AB.

Sundberg J, Back P-E, Ländell M, Sundberg A, 2009. Modelling of temperature in deep boreholes and evaluation of geothermal heat flow at Forsmark and Laxemar. SKB TR-09-14, Svensk Kärnbränslehantering AB.

Svensson U, Ferry M, Kuylenstierna H-O, 2010. DarcyTools version 3.4. Concepts, methods and equations. SKB R-07-38, Svensk Kärnbränslehantering AB.

Vidstrand P, 2003. Surface and subsurface conditions in permafrost areas – a literature review. SKB TR-03-06, Svensk Kärnbränslehantering AB.

Vidstrand P, Follin S, Zugec N, 2010. Groundwater flow modelling of periods with periglacial and glacial climate conditions – Forsmark. SKB R-09-21, Svensk Kärnbränslehantering AB.

Werner K, Sassner M, Johansson E, 2013. Hydrology and near-surface hydrogeology at Forsmark – synthesis for the SR-PSU project. SR-PSU Biosphere. SKB R-13-19, Svensk Kärnbränslehantering AB.

Williams P J, Smith M W, 1989. The frozen earth: fundamentals of geocryology. Cambridge: Cambridge University Press.

Öhman J, 2010. Site investigation SFR. Hydrogeologic modelling of SFR v 0.1. Influence of the ridge on the flow fields for different target volumes. SKB R-09-43, Svensk Kärnbränslehantering AB.

Öhman J, Bockgård N, Follin S, 2012. Site investigation SFR. Bedrock hydrogeology. SKB R-11-03, Svensk Kärnbränslehantering AB.

Öhman J, Follin S, Odén M, 2013. Site investigation SFR. Bedrock hydrogeology – Groundwater flow modelling. SKB R-11-10, Svensk Kärnbränslehantering AB.

Öhman J, Follin S, Odén M, 2014. SR-PSU Hydrogeological modelling. TD11 – Temperate climate conditions. SKB P-14-04, Svensk Kärnbränslehantering AB.

Unpublished documents

SKBdoc id, version	Title	Issuer, year
1395215 ver 1.0	TD10-SFR 3 adaptation to hydrogeological conditions	SKB, 2013

Appendix A

Task Description 13

Date	121010	121214	121218	120201
Version	0.01	0.03	0.04	0.05
Approved	MO			
Name of task	TH modelling of SFR PSU			
Code	DarcyTools v. 3.4			
Modeller	PV			

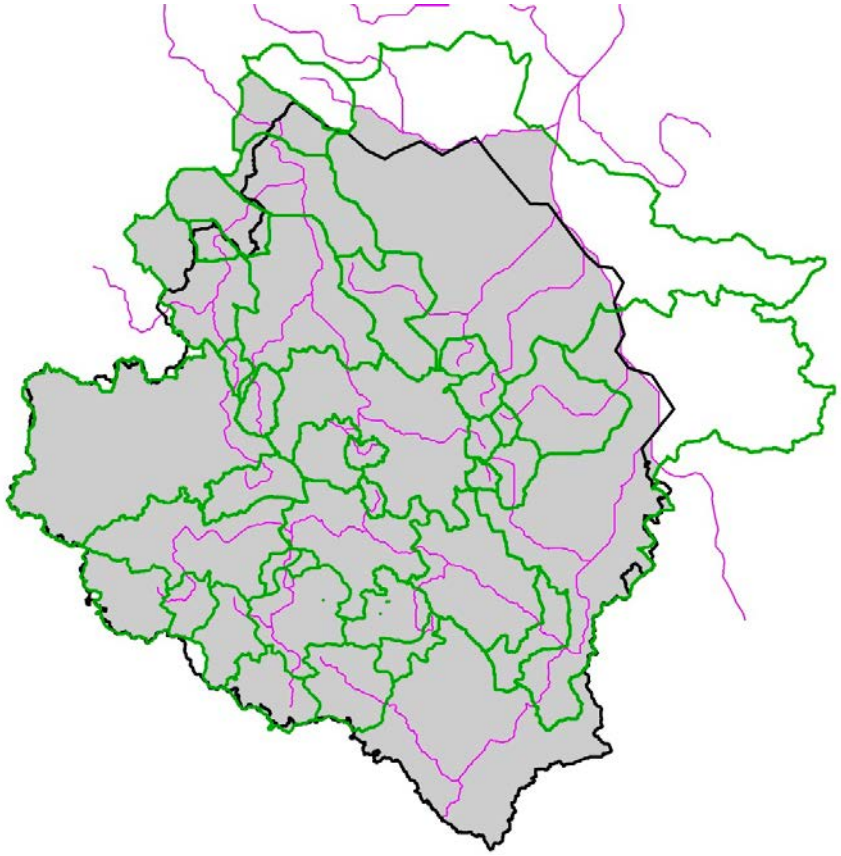

Updated flow domain (grey area = used in TD13, black line = used before TD11).

Scope of work

- Calculate through flow, total and local values, to SFR1 and L1BC layout using the SFR regional flow model area indicated in the illustration shown above.
- Calculate recharge- and discharge locations for particle traces passing through repository vaults in SFR1 and the L1BC layout using the SFR flow model area shown in illustration above.
- Calculate pressure field in the near-field of SFR. Calculate permafrost associated property changes in the near-field of SFR.
- Calculate relevant performance measures, e.g. Darcy fluxes, F, path length, and advective travel time.

The simulations should be TH(C) coupled and permafrost should be assessed so that the depth of frozen ground reach 1) elevations just above SFR1, 2) reach elevations between SFR1 and the L1BC layout, and 3) reach elevations below the entire extended SFR facility.

Bedrock Cases:

Case1: HCD_BASE_CASE1 and DFN case R85.

Case11: HCD_nc_DEP_R07 and DFN case R85.

Case15: HCD_nc_NoD_R01 and DFN case R18.

Flow Simulations:

Case1 a) permafrost above SFR1 b) permafrost between SFR1 and L1BC c) permafrost below SFR facility. In all three simulations taliks are defined based on rivers, lake and ponds by Lars Brydsten for 20,000 AD along with ponds created by MikeShe for 11,000 AD simulation.

Case12 a) permafrost above SFR1 b) permafrost between SFR1 and L1BC c) permafrost below SFR facility. In all three simulations taliks are defined based on rivers, lake and ponds by Lars Brydsten for 20,000 AD and the most upstream lakes from the MikeShe simulation to test a regional cross-flow only.

Case11 same as 1 above.

Case112 same as 12 above.

Case15 same as 1 above.

Case152 same as 12 above.

In total 18 simulations planned.

Deliverables

1) **Delivery to nearfiled in Comsol.**
   - To be defined.

2) **Delivery to Radionuclide transport modeling, Chemistry, and Biosphere. For each simulation a file containing at least the bullets below is delivered.**
   - **Wall__ID** = Tunnel-wall ID in the DT grid where the particle enters into the bedrock. Several particles may have the same tunnel-wall ID; the number of particles through a tunnel wall is proportional to outward-directed flow.
   - **Wall_q(m/s)** = Darcy flux, q (m/s), through a 2 m × 2 m section of the tunnel wall. Can be re-scaled into flow, Q (m^3/s), using area = 4 m^2.
   - **Release_X** = DT cell- wall centre x-coordinate of the release location at the tunnel wall of the disposal facility (RT90).
   - **Release_Y** = DT cell- wall centre y-coordinate of the release location at the tunnel wall of the disposal facility (RT90).
   - **Release_Z** = DT cell- wall centre z-coordinate of the release location at the tunnel wall of the disposal facility (RHB70, neglecting landlift since 1970).
   - **Time (s)** = cumulative residence time for particle, based on the kinematic porosity of [Bedrock case] as calculated in GEHYCO (min porosity = $1 \cdot 10^{-5}$).
   - **F-quot(s/m)** = cumulative F-quotient for trajectory, based on the flow-wetted surface area of [Bedrock case] as calculated in GEHYCO.
   - **FWS (m^2)** = cumulative flow-wetted surface area for trajectory, as calculated for the [Bedrock case] in GEHYCO.
   - **Exit_q(m/s)** = Darcy flux, q (m/s), through the bedrock/HSD interface; Can be re-scaled into flow, Q (m^3/s), using area A, specified below.
   - **A(m^2)** = cell-wall area for flux through the bedrock/HSD interface; provided to facilitate conversion into flow, Q (m^3/s).
   - **Exit____X** = DT cell-wall centre x-coordinate of the exit location, i.e. passing through the bedrock/HSD interface (RT90).

- **Exit____Y** = DT cell-wall centre y-coordinate of the exit location, i.e. passing through the bedrock/HSD interface (RT90).
- **Exit__Z** = Discretised z-coordinate of the exit location in the DT grid (RHB70, neglecting landlift since 1970); for a given (x,y) position, the *true* elevation of the bedrock/HSD interface is defined in RLDM.
- **Pathlength(m)** = Total length of flow path in the bedrock (m).
- **Cell_ID** = DT cell number in the last bedrock cell, prior to exit.

Background

Periods with periglacial climate conditions are hypothesized to have been primarily governed by the presence of permafrost reaching varying depths. The freezing of the ground significantly alters the hydrogeological properties of the ground materials, regolith as well as bedrock. In order to account for these changes, the numerical model needs to address thermal processes and account for thermally driven changes, in particular changes in the permeability.

Suggested conceptual model

A groundwater flow model intended for periglacial climate conditions have different material properties and boundary conditions than those currently prevailing. With regard to the four bullets listed in the scope of work section above, the suggested conceptual model is as follows.

The flow beneath the permafrost depth is significantly reduced since the recharge from above is almost “cut-off” by the frozen ground. In addition, all other boundaries are modelled as no-flow. Thus, the locations, extent and amount of taliks control the flow field within the model domain.

A super-regional groundwater gradient may be of the order of 0.001 m/m based on future sea levels and large enough lakes that may survive a landscape evolution in the area up to the plausible first occurring permafrost incident some 15,000 years from now. A local groundwater gradient imposed by small taliks inside the model domain may be in the same range but possible some 2–5 times larger, since the talik locations correlates with local topography.

Two future talik lakess occur in the lowest part of the model domain at 20,000 AD (delivered by Lars Brydsten), see green coloured locations in figure below. However, since the elevations of the two taliks are just about equal and their locations are close to each other and on the boundary, there will be almost no flow beneath the frozen ground in the main part of the model domain unless the no-flow vertical boundaries are changed to open boundaries, e.g. by assigning a regional groundwater flux/gradient.

An alternative is to use a talik situation derived from e.g. a MIKE SHE simulation, which produces more potential talik locations of smaller size since Lars Brydsten’s model neglects small ponds/shallows.

In SR-Site, MIKE SHEe produced a talik distribution for a permafrost depth of 100 metres and 250 metres (Bosson et al. 2010) based on SR-Site’s regolith model, the 10,000 AD DEM, and surface hydraulic situation. The 100 metres thick permafrost case produces a significant amount of local taliks within the assessed model domain, A similar data set (in shape files) based on the present SR-PSU information for 11,000 AD (delivered by Emma Bosson) will be assessed (see red coloured locations in figure below).

Using this situation as a top-boundary condition will show a possible extreme as of “high” fluxes in the model, the uncertainty apparent in results due to omission of a super-regional flow gradient is possibly hence much smaller.

The suggested strategy is to assess the second alternative as the base case and the first case including an estimate (as of direction and magnitude) of a regional gradient as a variant case.

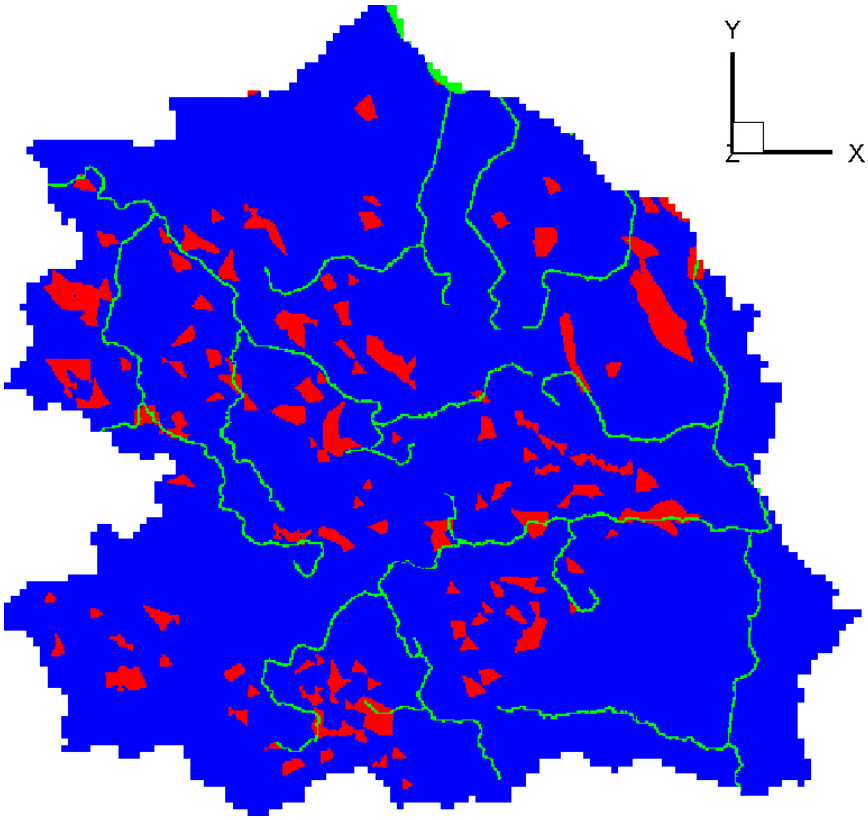

Prerequisites

Geometrical description

- Surface water divides. File used: R_Updated_WD_model_domain.dat
- Tunnel layout
  - SFR1:
  - L1BC:
- DEM for 20,000 AD. Geometry of DEM from delivery by L Brydsten, 2012-10-09 11:24. Files modified to DT format by P Askling, Geosigma.
- The flow domain is approximately cut at an elevation of –1,000 metres.

Material properties

Simulations are planned to be done with a couple of different realisations of fracture network and deformation zone settings. The amount of realisations assessed will depend on the available time.

For a first Base case set up:

SFR regional model domain

- HCD from SDM-PSU. File used: R_Param_SFR_HCD_BASE_CASE1.
- SBA from SDM-PSU. File used: R_Parameterized_SFR_SBA1_to_SBA8.
- PDZ from SDM- PSU. File used: R_Unresolved_PDZ_R85_knwn.
- HRD from SDM-PSU. File used: R_SFR_DFN_connected_R85_knwn.
- HSD from SDM-Site / SR-Site: Data used are based on information found in Bosson et al. (2010).

Other areas

- HCD from SDM-Site / SR-Site. File used: R_PFM_zoner_med_hl_i_mitten and R_ Parameterized_SFR_BRIDGES.
- HRD from SR-Site's "Heterogeneity Case" (Joyce et al. 2010). File used: R_UPDATED_ SERCO_DFN_WITH_HOLE.
- HSD from SDM-Site / SR-Site: Data used are based on information found in Bosson et al. (2010).
- Sheet joints from SDM-Site / SR-Site. File used: R_PLU_sheet_joints_truncated.
- Surface hydrology (lakes and rivers) from L Brydsten or E Bosson. Geometry of future lakes and rivers at 20,000 AD from delivery by L Brydsten, 2012-10-09 11:24. Files modified to DT format by P Askling, Geosigma. Alternative lake/talik geometries from delivery by E Bosson, 2013-01-17 11:08 (11,000 AD).
- Tunnel backfill materials. Tunnel backfill materials based on SKB (2014c).

Additional properties

- Porosity for the bedrock derived from the free volume calculated within DT. Each fracture is given a specific width based on a width-tranmissivity relationship, $e_T = 0.46 \cdot T^{0.5}$, as stated in Dershowitz et al. (2003).
- Porosity for regoliths based on information found in Bosson et al. (2010).
- FWS for the bedrock calculated within DT using standard algorithm within DT.
- FWS for regoliths based on information taken from Maxe (2003).
- Thermal properties taken from Hartikainen et al. (2010) and Vidstrand et al. (2010).
- Simulation assume pseudo-steady-state, Specific storage hence set to zero.

Coordinate system

- RT90 with a local origo set at (1626000, 6692000).
- Rotated.

Processes and couplings

- Coupling of Mass, (Salt) and Heat equations.
- Permeability changes.

Boundary conditions and intrinsic state conditions

- Future shoreline locations relevant for the investigated time period. Taken from FM_SM_ shoreequations_2007_AD.xls.
- Specified pressure following land cells.
- Specified pressure taken as lake elevations on lake cells.
- Assessed annual mean ground surface temperature on land cells needed to create the permafrost depths assessed.
- Annual mean temperature of 4 Degrees Centigrade on sea and lake cells.
- Specified heat flux at bottom boundary. Taken from Vidstrand et al. (2010).
- No-flow lateral boundaries and bottom boundary: Bottom no-flow boundary motivated by low deep flow and shallow SFR location. Lateral no-flow boundary taken as topographical surface-water divides.

- SFR facilities operating under backfilled and re-saturated conditions. The plugs will be intact for the permafrost cases but a simulation with broken down plugs will be conducted for parts that has been frozen in each case.
- Saline water conditions (only for a possible glacial scenario).
  - Salt initiated as specified in SDM Site.
  - Salinity and shore level in Baltic Sea according to extrapolated curves presented in Joyce et al. (2010).
  - Fresh water recharge on land cells.
  - Salinity development simulated up to starting point for THC simulations at the first freezing event in the Early Periglacial scenario.
- Minimum conductivity used instead of cell deletion. All cell-face conductivities $< 3 \cdot 10^{-11}$ m/s resulting from GEHYCO are assigned the value $3 \cdot 10^{-11}$ m/s.

Calibration targets

- None.

Calibration knob

- None.

Output

- Through flow for repository vaults within SFR1 and the L1BC layout before, during and after the period of frozen ground. For after the period of frozen ground both intact and broken down plugs will be assessed.
- Recharge and discharge locations. Method used: cell-jump particle tracking technique.
- Particle transport parameters (porosity, path length, Darcy flux and F-factor) to be delivered to Per-Gustav Åstrand for use in transport calculations.
- Pressure field in the near-field of rock vaults to be delivered to Amphos for simulations of inside rock vaults flow in Comsol.

Suggested QA

- Check of prpgen: Johan Öhman.
- Check of fif: Johan Öhman.
- Check of thermal properties: Jan Sundberg.
- The QA is following the QA programme of TerraSolve AB.
- All input and output files will be stored according to TerraSolve AB:s QA system and will on request be delivered to SKB.

Suggested sensitivity comparisons

- Check of assessed temperatures and related permafrost depths reached with results by Hartikainen et al. (2010).
- Check effect on fluxes if possible local small taliks are omitted.

Appendix B

Table B-1. Used tunnel/tunnel plug geometry. Source data related to data delivery at Project Place (PP): _24_SFR_STL_121220.

Source data (CAD format)
SFR1_1BTF_del1_yellow.stl
SFR1_2BTF_del1_yellow.stl
SFR1_1BLA_del1_yellow.stl
SFR1_1BMA_del1_yellow.stl
SFR1_Silo_del1_topp_yellow.stl
SFR1_Silo_del2_under_topp_yellow.stl
SFR1_Silo_del3_yttre_yellow.stl
SFR1_Silo_del4_mitt_yellow.stl
SFR1_Silo_del5_undre_yellow.stl
L1BC_1BRT_del1_yellow.stl
L1BC_2BLA_del1_yellow.stl
L1BC_3BLA_del1_yellow.stl
L1BC_4BLA_del1_yellow.stl
L1BC_5BLA_del1_yellow.stl
L1BC_2BMA_del1_yellow.stl
SFR1_1BT_del1_white.stl
SFR1_1BT_del2_white.stl
SFR1_1BT_del3_white.stl
SFR1_1BT_del4_genomstick_white.stl
SFR1_1BT_del5_white.stl
SFR1_1BT_del7_white.stl
SFR1_1BT_del9_white.stl
SFR1_1BT_del10_genomstick_white.stl
SFR1_1BT_del11_white.stl
SFR1_1BT_del12_white.stl
SFR1_1BT_del13_nedre_stick_white.stl
SFR1_1BT_del14_nedre_stick_white.stl
SFR1_1BT_del15_white.stl
SFR1_1BT_del16_white.stl
SFR1_1BT_del17_white.stl
SFR1_1BT_del18_white.stl
SFR1_1BT_del19_white.stl
SFR1_1BT_del20_white.stl
SFR1_1BT_del26_white.stl
SFR1_1BT_del27_white.stl
SFR1_1BT_del28_white.stl
SFR1_1BT_del34_white.stl
SFR1_1BT_del35_anslutning_schakt_white.stl
SFR1_1BT_del36_undre_del_white.stl
SFR1_1BT_del37_undre_del_white.stl
SFR1_1BT_del38_undre_del_white.stl
SFR1_1BT_del39_undre_del_white.stl
SFR1_1BT_del40_undre_del_white.stl
SFR1_1BT_del53_undre_del_white.stl
SFR1_1BT_del54_undre_del_schakt_white.stl
SFR1_1DT_del1_white.stl

Source data (CAD format)
SFR1_1DT_del2_white.stl
SFR1_1DT_del3_white.stl
SFR1_1DT_del4_white.stl
SFR1_1DT_del5_white.stl
SFR1_1DT_del6_white.stl
SFR1_1DT_del7_white.stl
SFR1_1DT_del8_white.stl
SFR1_1DT_del11_white.stl
SFR1_1DT_del12_white.stl
SFR1_1DT_del15_white.stl
SFR1_1DT_del16_white.stl
SFR1_1DT_del17_white.stl
SFR1_1DT_del18_white.stl
SFR1_1DT_del19_white.stl
SFR1_1DT_del20_white.stl
SFR1_1DT_del21_white.stl
SFR1_1DT_del22_white.stl
SFR1_1DT_del23_white.stl
SFR1_1DT_del24_white.stl
SFR1_1DT_del25_white.stl
SFR1_1DT_del26_white.stl
SFR1_1DT_del27_white.stl
SFR1_1DT_del28_white.stl
SFR1_1DT_del29_white.stl
L1BC_1BST_del1_white.stl
L1BC_1RTT_del1_white.stl
L1BC_1RTT_del2_white.stl
L1BC_1RTT_del3_white.stl
L1BC_1RTT_del4_white.stl
L1BC_1RTT_del6_white.stl
L1BC_1RTT_del8_white.stl
L1BC_1RTT_del9_white.stl
L1BC_1RTT_del10_white.stl
L1BC_1RTT_del11_white.stl
L1BC_1RTT_del12_white.stl
L1BC_1RTT_del13_white.stl
L1BC_1RTT_del14_white.stl
L1BC_1TIT_del1_white.stl
L1BC_1TIT_del2_white.stl
L1BC_1TIT_del3_white.stl
L1BC_1TIT_del4_white.stl
L1BC_2DT_del1_white.stl
L1BC_2DT_del2_white.stl
L1BC_2DT_del3_white.stl
L1BC_2DT_del4_white.stl
L1BC_2DT_del5_white.stl
L1BC_2TT_del4_white.stl

Source data (CAD format)
SFR1_1BT_del21_silotunnel_blue_plugg.stl
SFR1_1BT_del29_blue_plugg.stl
SFR1_1BT_del33_blue_plugg.stl
SFR1_1BT_del41_undre_del_blue_plugg.stl
SFR1_1BT_del52_undre_del_blue_plugg.stl
SFR1_1BTF_ut_del2_blue_plugg.stl
SFR1_1BTF_ut_del4_blue_plugg.stl
SFR1_1TT_del1_blue_plugg.stl
SFR1_1TT_del10_blue_plugg.stl
SFR1_1TT_del4_blue_plugg.stl
SFR1_1TT_del7_blue_plugg.stl
L1BC_1BST_del2_blue_plugg.stl
L1BC_1IN_del2_blue_plugg.stl
L1BC_1RTT_del15_blue_plugg.stl
L1BC_1UT_del2_blue_plugg.stl
L1BC_2IN_del2_blue_plugg.stl
L1BC_2TT_del3_blue_plugg.stl
L1BC_2UT_del2_blue_plugg.stl
L1BC_3IN_del2_blue_plugg.stl
L1BC_3UT_del2_blue_plugg.stl
L1BC_4IN_del2_blue_plugg.stl
L1BC_4UT_del2_blue_plugg.stl
L1BC_5IN_del2_blue_plugg.stl
L1BC_5UT_del2_blue_plugg.stl
L1BC_6IN_del2_blue_plugg.stl
L1BC_6UT_del2_blue_plugg.stl
SFR1_1BST_del4_brown_plugg.stl
SFR1_1BST_del6_brown_plugg.stl
SFR1_1BST_del7_brown_plugg.stl
SFR1_1BST_del8_brown_plugg.stl
SFR1_1BST_del10_brown_plugg.stl
SFR1_1BST_del11_brown_plugg.stl
SFR1_1BST_del12_brown_plugg.stl
SFR1_1BST_del14_brown_plugg.stl
SFR1_1BST_del15_brown_plugg.stl
SFR1_1BST_del16_brown_plugg.stl
SFR1_1BST_del18_brown_plugg.stl
SFR1_1BST_del19_brown_plugg.stl
SFR1_1BT_del22_silotunnel_brown_plugg.stl
SFR1_1BT_del23_silotunnel_brown_plugg.stl
SFR1_1BT_del24_silotunnel_brown_plugg.stl
SFR1_1BT_del25_silotunnel_brown_plugg.stl
SFR1_1BT_del30_brown_plugg.stl
SFR1_1BT_del31_brown_plugg.stl
SFR1_1BT_del32_brown_plugg.stl
SFR1_1BT_del42_undre_del_brown_plugg.stl
SFR1_1BT_del43_undre_del_brown_plugg.stl
SFR1_1BT_del44_undre_del_brown_plugg.stl
SFR1_1BT_del45_undre_del_brown_plugg.stl
SFR1_1BT_del46_undre_del_brown_plugg.stl
SFR1_1BT_del47_undre_del_brown_plugg.stl
SFR1_1BT_del48_undre_del_brown_plugg.stl
SFR1_1BT_del49_undre_del_brown_plugg.stl
SFR1_1BT_del50_undre_del_brown_plugg.stl
SFR1_1BT_del51_undre_del_brown_plugg.stl

Source data (CAD format)
SFR1_1BTF_ut_del3_brown_plugg.stl
SFR1_1TT_del2_brown_plugg.stl
SFR1_1TT_del3_brown_plugg.stl
SFR1_1TT_del5_brown_plugg.stl
SFR1_1TT_del6_brown_plugg.stl
SFR1_1TT_del8_brown_plugg.stl
SFR1_1TT_del9_brown_plugg.stl
SFR1_1TT_del11_brown_plugg.stl
SFR1_1TT_del12_brown_plugg.stl
L1BC_1BST_del3_brown_plugg.stl
L1BC_1BST_del4_brown_plugg.stl
L1BC_1IN_del1_brown_plugg.stl
L1BC_1UT_del1_brown_plugg.stl
L1BC_2IN_del1_brown_plugg.stl
L1BC_2NDB_del1_brown_plugg.stl
L1BC_2TT_del1_brown_plugg.stl
L1BC_2TT_del2_brown_plugg.stl
L1BC_2UT_del1_brown_plugg.stl
L1BC_3IN_del1_brown_plugg.stl
L1BC_3NDB_del1_brown_plugg.stl
L1BC_3UT_del1_brown_plugg.stl
L1BC_4IN_del1_brown_plugg.stl
L1BC_4UT_del1_brown_plugg.stl
L1BC_5IN_del1_brown_plugg.stl
L1BC_5UT_del1_brown_plugg.stl
L1BC_6IN_del1_brown_plugg.stl
L1BC_6UT_del1_brown_plugg.stl
SFR1_1BST_del1_green_plugg.stl
SFR1_1BST_del2_green_plugg.stl
SFR1_1BST_del3_green_plugg.stl
SFR1_1BST_del5_green_plugg.stl
SFR1_1BST_del9_green_plugg.stl
SFR1_1BST_del13_green_plugg.stl
SFR1_1BST_del17_green_plugg.stl
SFR1_1BT_del6_pink_plugg.stl
SFR1_1BT_del8_pink_plugg.stl
SFR1_1DT_del9_pink_plugg.stl
SFR1_1DT_del10_pink_plugg.stl
SFR1_1DT_del13_pink_plugg.stl
SFR1_1DT_del14_pink_plugg.stl
L1BC_1RTT_del5_pink_plugg.stl
L1BC_1RTT_del7_pink_plugg.stl

Table B-2. Used tunnel/tunnel plug geometry. Constructed input data related to the source data from delivery at Project Place (PP): _24_SFR_STL_121220.

Rotated DarcyTools object
R_1BTF_del1_yellow.dat
R_2BTF_del1_yellow.dat
R_1BLA_del1_yellow.dat
R_1BMA_del1_yellow.dat
R_Silo_del1_topp_yellow.dat
R_Silo_del2_under_topp_yellow.dat
R_Silo_del3_yttre_yellow.dat
R_Silo_del4_mitt_yellow.dat
R_Silo_del5_undre_yellow.dat
R_1BRT_del1_yellow.dat
R_2BLA_del1_yellow.dat
R_3BLA_del1_yellow.dat
R_4BLA_del1_yellow.dat
R_5BLA_del1_yellow.dat
R_2BMA_del1_yellow.dat
R_1BT_del1_white.dat
R_1BT_del2_white.dat
R_1BT_del3_white.dat
R_1BT_del4_genomstick_white.dat
R_1BT_del5_white.dat
R_1BT_del7_white.dat
R_1BT_del9_white.dat
R_1BT_del10_genomstick_white.dat
R_1BT_del11_white.dat
R_1BT_del12_white.dat
R_1BT_del13_nedre_stick_white.dat
R_1BT_del14_nedre_stick_white.dat
R_1BT_del15_white.dat
R_1BT_del16_white.dat
R_1BT_del17_white.dat
R_1BT_del18_white.dat
R_1BT_del19_white.dat
R_1BT_del20_white.dat
R_1BT_del26_white.dat
R_1BT_del27_white.dat
R_1BT_del28_white.dat
R_1BT_del34_white.dat
R_1BT_del35_ansl_schakt_white.dat
R_1BT_del36_undre_del_white.dat
R_1BT_del37_undre_del_white.dat
R_1BT_del38_undre_del_white.dat
R_1BT_del39_undre_del_white.dat
R_1BT_del40_undre_del_white.dat
R_1BT_del53_undre_del_white.dat
R_1BT_del54_undre_del_sch_white.dat
R_1DT_del1_white.dat
R_1DT_del2_white.dat
R_1DT_del3_white.dat
R_1DT_del4_white.dat
R_1DT_del5_white.dat
R_1DT_del6_white.dat
R_1DT_del7_white.dat

Rotated DarcyTools object
R_1DT_del8_white.dat
R_1DT_del11_white.dat
R_1DT_del12_white.dat
R_1DT_del15_white.dat
R_1DT_del16_white.dat
R_1DT_del17_white.dat
R_1DT_del18_white.dat
R_1DT_del19_white.dat
R_1DT_del20_white.dat
R_1DT_del21_white.dat
R_1DT_del22_white.dat
R_1DT_del23_white.dat
R_1DT_del24_white.dat
R_1DT_del25_white.dat
R_1DT_del26_white.dat
R_1DT_del27_white.dat
R_1DT_del28_white.dat
R_1DT_del29_white.dat
R_1BST_del1_white.dat
R_1RTT_del1_white.dat
R_1RTT_del2_white.dat
R_1RTT_del3_white.dat
R_1RTT_del4_white.dat
R_1RTT_del6_white.dat
R_1RTT_del8_white.dat
R_1RTT_del9_white.dat
R_1RTT_del10_white.dat
R_1RTT_del11_white.dat
R_1RTT_del12_white.dat
R_1RTT_del13_white.dat
R_1RTT_del14_white.dat
R_1TIT_del1_white.dat
R_1TIT_del2_white.dat
R_1TIT_del3_white.dat
R_1TIT_del4_white.dat
R_2DT_del1_white.dat
R_2DT_del2_white.dat
R_2DT_del3_white.dat
R_2DT_del4_white.dat
R_2DT_del5_white.dat
R_2TT_del4_white.dat
R_1BT_del21_silotunnel_blue.dat
R_1BT_del29_blue_plugg.dat
R_1BT_del33_blue_plugg.dat
R_1BT_del41_undre_del_blue.dat
R_1BT_del52_undre_del_blue.dat
R_1BTF_ut_del2_blue.dat
R_1BTF_ut_del4_blue.dat
R_1TT_del1_blue.dat
R_1TT_del10_blue.dat
R_1TT_del4_blue.dat
R_1TT_del7_blue.dat

Rotated DarcyTools object
R_1BST_del2_blue.dat
R_1IN_del2_blue.dat
R_1RTT_del15_blue.dat
R_1UT_del2_blue.dat
R_2IN_del2_blue.dat
R_2TT_del3_blue.dat
R_2UT_del2_blue.dat
R_3IN_del2_blue.dat
R_3UT_del2_blue.dat
R_4IN_del2_blue.dat
R_4UT_del2_blue.dat
R_5IN_del2_blue.dat
R_5UT_del2_blue.dat
R_6IN_del2_blue.dat
R_6UT_del2_blue.dat
R_1BST_del4_SFR1_brown.dat[1)]
R_1BST_del6_brown.dat
R_1BST_del7_brown.dat
R_1BST_del8_brown.dat
R_1BST_del10_brown.dat
R_1BST_del11_brown.dat
R_1BST_del12_brown.dat
R_1BST_del14_brown.dat
R_1BST_del15_brown.dat
R_1BST_del16_brown.dat
R_1BST_del18_brown.dat
R_1BST_del19_brown.dat
R_1BT_del22_silotunnel_brown.dat
R_1BT_del23_silotunnel_brown.dat
R_1BT_del24_silotunnel_brown.dat
R_1BT_del25_silotunnel_brown.dat
R_1BT_del30_brown_plugg.dat
R_1BT_del31_brown_plugg.dat
R_1BT_del32_brown_plugg.dat
R_1BT_del42_undre_del_brown.dat
R_1BT_del43_undre_del_brown.dat
R_1BT_del44_undre_del_brown.dat
R_1BT_del45_undre_del_brown.dat
R_1BT_del46_undre_del_brown.dat
R_1BT_del47_undre_del_brown.dat
R_1BT_del48_undre_del_brown.dat
R_1BT_del49_undre_del_brown.dat
R_1BT_del50_undre_del_brown.dat
R_1BT_del51_undre_del_brown.dat
R_1BTF_ut_del3_brown.dat
R_1TT_del2_brown.dat
R_1TT_del3_brown.dat
R_1TT_del5_brown.dat
R_1TT_del6_brown.dat
R_1TT_del8_brown.dat
R_1TT_del9_brown.dat
R_1TT_del11_brown.dat
R_1TT_del12_brown.dat

Rotated DarcyTools object
R_1BST_del3_brown.dat
R_1BST_del4_L1BC_brown.dat[1)]
R_1IN_del1_brown.dat
R_1UT_del1_brown.dat
R_2IN_del1_brown.dat
R_2NDB_del1_brown.dat
R_2TT_del1_brown.dat
R_2TT_del2_brown.dat
R_2UT_del1_brown.dat
R_3IN_del1_brown.dat
R_3NDB_del1_brown.dat
R_3UT_del1_brown.dat
R_4IN_del1_brown.dat
R_4UT_del1_brown.dat
R_5IN_del1_brown.dat
R_5UT_del1_brown.dat
R_6IN_del1_brown.dat
R_6UT_del1_brown.dat
R_1BST_del1_green.dat
R_1BST_del2_green.dat
R_1BST_del3_green.dat
R_1BST_del5_green.dat
R_1BST_del9_green.dat
R_1BST_del13_green.dat
R_1BST_del17_green.dat
R_1BT_del6_pink_plugg.dat
R_1BT_del8_pink_plugg.dat
R_1DT_del9_pink.dat
R_1DT_del10_pink.dat
R_1DT_del13_pink.dat
R_1DT_del14_pink.dat
R_1RTT_del5_pink.dat
R_1RTT_del7_pink.dat

1) Owing to an inconsistency in delivered file names, the objects must be differentiated by means of specification to ”SFR1” or ”L1BC”.